Oxygen-induced segregation during batch annealing of industrial steel coils

By

Etienne Wurth

A dissertation submitted in
fulfilment of the requirements for the degree of

MAGISTER SCIENTIAE

Department of Physics
Faculty Natural & Agricultural Sciences
University of the Free State

Supervisor: Prof. HC Swart
Co-Supervisor: Prof. JJ Terblans

May 2006

To my father

Gerhard Hellmut Wurth

Acknowledgements

The author wishes to express his thanks and gratitude to the following people:

- *Prof HC Swart*, for all his patience and motivation during this study
- *Prof JJ Terblans,* for all his assistance with the computers and apparatus
- *Mr. AB Hugo and the personnel of the Electronics division*, for their maintenance on the electronic systems
- *Mr. R Veltman and the personnel of the Instrumentation division*, for their technical support
- *The personnel of the Physics Department*, for their kindness and for numerous informative conversations
- *All my friends*, for all there support
- *My parents and family*, for their unending support
- *Mr. HD Joubert*, for his assistance with temperamental computers

Abstract

The development of diffusion welds between spirals of steel coils, during batch annealing, is of particular interest because it prevents the coils from being unwound for further use. The physical metallurgy of iron and steel is exceedingly complicated and many of the complications arise from the behaviour of solutes, which segregate to surfaces and interfaces, which alter the mechanical behaviour.

Segregation studies were done by measuring the APPH's (Auger Peak to Peak Heights) of the segregating species (P, S, C and Ti) against annealing time during the annealing of an ultra low carbon (ULC) Ti stabilized steel between 550 and 800^{o}C. The modified Darken model was used to describe the complex segregation behaviour of the species involved during annealing of the industrial steel. This was done by comparing the initial changes in fractional surface concentration of the segregating species against annealing time to the trends in the surface concentration changes as describe by the Darken model for a ternary alloy. Calculations were done, using Langmuir-McClean equations, to determine the change in effective segregation energy as a function of oxygen surface coverage.

Oxidation was allowed after sputtered cleaning and segregation, these oxidation results were compared with each other. No C segregation occurred without oxygen in the system. Oxygen induced-segregation of Ti and C occurred at 700^{o}C and 800^{o}C. Oxidation occurred at 700^{o}C and 800^{o}C. It was found that the adsorption of oxygen on the surface profoundly influence the segregation rate of the species involved.

The modified Darken model was successfully used to describe the oxygen induced-segregation process. The induced segregation may act as a possible source of the diffusion welds during batch annealing.

Key Words

Oxidation
Segregation
Auger Electron Spectroscopy (AES)
Diffusion
Langmuir-McClean equation
Darken Model
Segregation Energy
Linear Least Squares (LLS)
Industrial Steel
Oxygen Induced Segregation

Table of Contents

Chapter 1

Introduction

During the production of flat steel, a significant amount of work hardening takes place when the steel is rolled up into coils, for storing purpose. These steel coils are batch annealed in order to reduce the hardness and restore formability, before further production takes place. The development of diffusion welds between layers of the steel coils, during batch annealing, is of particular interest because it prevents the coils from being unwind for further use. This problem is often referred to as strip adhesion or stickering. In a typical batch annealing process, several coils are annealed in a bell-shaped furnace (as shown in figure 1.1) and a reducing gas, i.e. hydrogen or nitrogen/hydrogen mixture, is passed through the coils, in a circular fashion, to remove rolling oils and prevent oxidation [1]. The heat is supplied from outside the inner cover by means of a heater that covers the system.

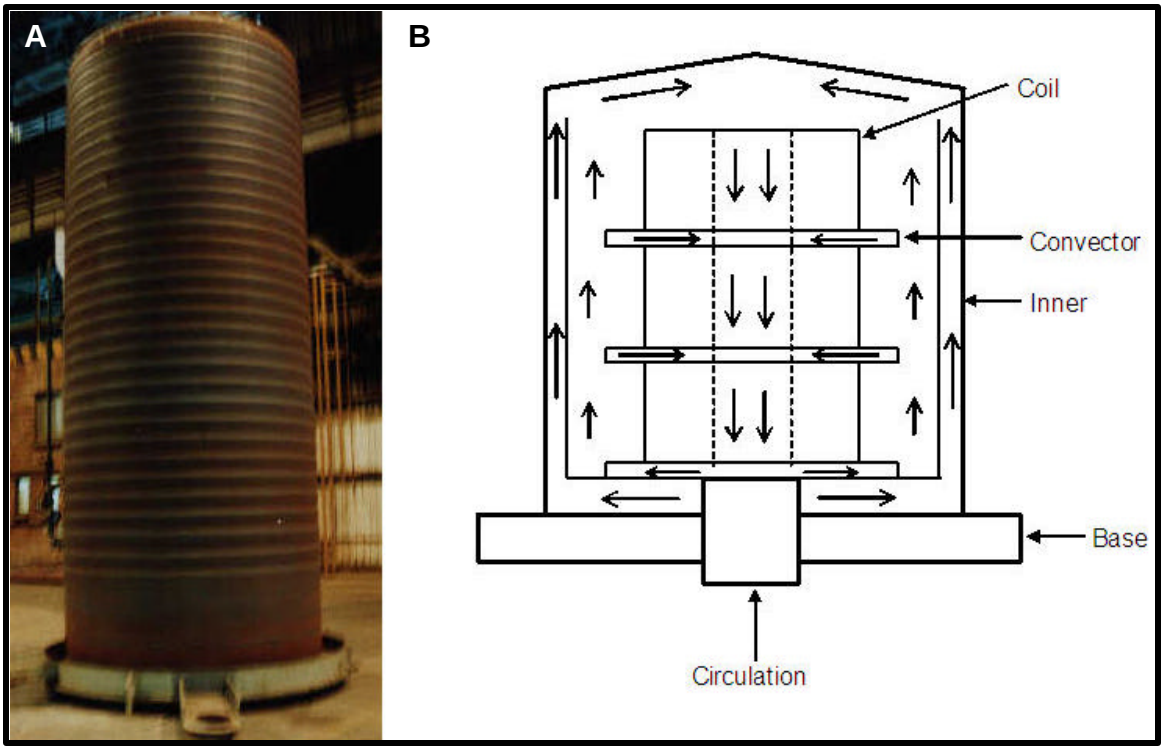

Figure 1.1: A - Photo of bell-shaped furnace. B - Illustration of the inside of the furnace.

During the batch annealing process, heating occurs in the form of a temperature ramp, which increases to a maximum temperature of about 670°C before decreasing it to room temperature. According to experimental findings, strip adhesion usually takes place at the critical time interval shown on the temperature ramp in figure 1.2 [2].

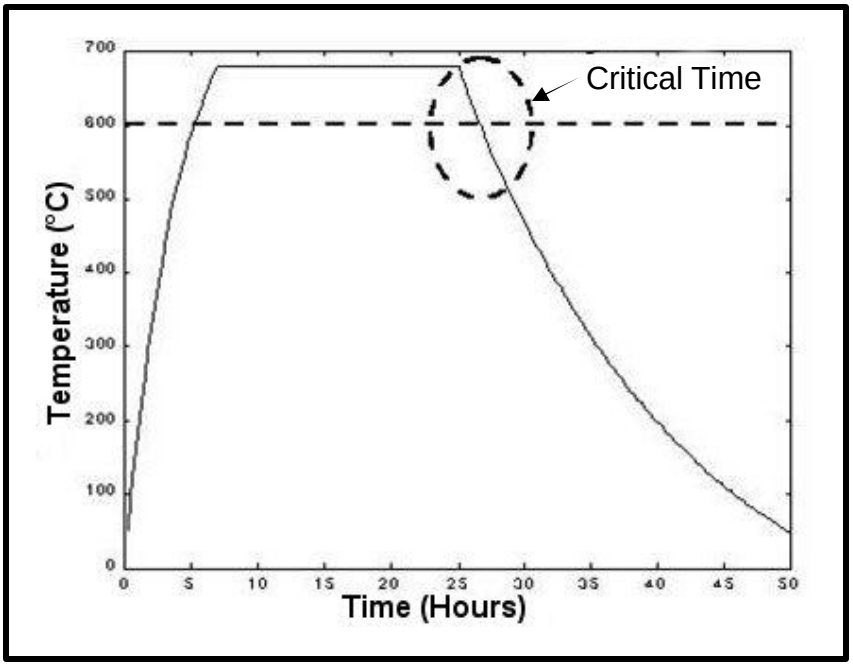

Figure 1.2: A typical temperature ramp with an indicated critical time interval. The coil spirals surface oxidizes at temperatures above 600^{o}C in the heating phase and reduction takes place on the surface below 600^{o}C, in the cooling phase.

The critical time interval is characterised by a steep decreasing thermal gradient and high thermal stresses. The Defox Plus process, which was developed by Peter Zylla [1], claims to prevent strip adhesion by circulating a gas mixture, during batch annealing, that oxidizes the coil spirals at temperatures above 600°C in the heating phase and reduces the coils below 600°C, in the cooling phase. This process was designed in such a way that an oxide layer is present on the spirals during the critical time interval, in order to discourage adhesion. After undergoing reduction, the coils emerge as desired.

Surface segregation is regarded as the redistribution of solute atoms between the surface and the bulk of a material resulting in an increase of the solute surface concentration, which is generally higher than the solute bulk concentration. Today surface segregation investigations have been applied in

many aspects [3], for example, the study of brittle fractures; grain-boundary diffusion and motion; the environmental effects such as intergranular corrosion and stress corrosion cracking; especially in the catalytic field.

The ultra low carbon (ULC) or interstitial free (IF) steels are typically used for both body structure and inner and outer body panels in the production of motor vehicles. Depending on what the steel is used for the steel must have adequate levels of formability, strength and weldability. There are two types of IF steels, the first are a highly formable steels with an yield strength close to 150 MPa and the second a high strength with a yield strength of about 250 MPa. To achieve the higher strength is by solid solution strengthening, usually by phosphorus [4,5].

The success of these steels depends on the proper solute carbon content. The solute carbon content for the low strength, high formability should be near zero, since solute carbon is damaging to texture formation during annealing and cold rolling. The production of steel components with set properties and uniformity relies on the precise disposition of carbon between particles and matrix. The bulk carbon content demands complete stabilization. To stabilize IF steels with C, N and S there must be added a microalloying element as titanium or niobium [4,5].

In Ti-containing steel the stabilization of C depends on the amount of Mn and S in the steel. In a commercial ULC steels the minimum bulk concentration is fixed by steelmaking, but the amount of S can vary. There should be an optimum combination of S and Ti, because if Ti concentration is to high surface defects can form [4]. In the Ti-IF steels the C, S and N form precipitates, these precipitates leads to the elimination of C, S and N elements from the solid solution [6].

The use of microalloying in the automotive components is the temperature dependent solubility of the microalloying elements as determined by the reaction

between N, C and the microalloying elements. Precipitates of Ti are increasingly stable with an increase in temperature. For TiN which is stable at 1200 C makes it possible for austenite grain size control at high forging temperatures [5].

The interactions of the segregated impurity species with metal and oxide surfaces are of significance to the oxidation and reduction stages since the presence of impurity elements, especially S, at the metal-oxide interface is associated with the instability of oxide over layers and the spallation of the oxide at high temperatures [7]. Holtzhausen and Roux [8] studied the segregation of S in an Fe-40Cr alloy and found that above 700°C the amount of S on the surface increases dramatically. Tjong and Swart [9] came to the same conclusion for an Fe-26Mn-7Al-0.9C alloy above 800°C where no oxidation could take place due to presence of this segregation layer. Van Staden and Roux [10] heated an Fe-40Cr alloy to 675°C, cooled it to room temperature and oxidised it at 440°C. The amount of S on the surface decreased, possibly due to the desorption as SO_2 gas.

1.1 Aim of Study

The purpose of this study is to show the influence of oxygen pressure on the complex segregation behaviour during the annealing of the industrial ULC steel. This is done by comparing the initial changes in APPH's (Auger Peak to Peak Heights) of the segregating species against annealing time with the trends in the surface concentration. The oxidation profiles taken place after sputter cleaning and after allowing segregation was also compared with each other. During oxidation the low energy Auger peak of Fe shifts several electron volts [16] and was therefore used to determine whether oxidation occurred during oxygen exposure.

1.2 Scope of Thesis

Chapter 2: A quick overview of the theory behind diffusion, is needed to understand segregation better. Fick's diffusion laws and the movement of atoms through the bulk forms the main part of this chapter.

Chapter 3: Discusses the theory behind segregation. The derivation of Fick's semi-infinite solution for segregating atoms is shown, but due to the driving force in his theory it is not possible to predict the equilibrium conditions. The modified Darken model is also discussed in this chapter.

Chapter 4: This chapter is an overview of the phenomena known as oxidation, especially iron oxides. The effect of oxidation has on segregation is investigated in order to link chapter 3 and 4.

Chapter 5: The experimental setup is discussed in more detail, with a look into Scanning Auger Microscopy (SAM) and the procedure used during this study. Additional information on special added equipment to the system is examined and a short discussion on the process to quantify the data is given.

Chapter 6: A discussion of the three basic parts of the experimental results obtained during the study, namely:

- The dependence of oxygen-induced segregation on the temperature.
- The influence of oxygen pressure on oxygen-induced segregation.
- The proposed theoretical model for the oxygen-induced segregation system.

Chapter 7: A conclusion is given, with possibilities of future work on this system.

Chapter 2

Diffusion

2.1 Introduction

Diffusion is the movement of atoms within a material. Atoms move in a predictable manner to eliminate concentration differences and produce a homogeneous, uniform composition [13].

The movement of atoms plays an essential role in the manufacturing of materials and the change of properties in materials, for example the heat treatment of metals, the production of ceramics and the manufacturing of electronic components such as transistors and solar cells.

In this chapter the basic idea of diffusion will be discussed, where there are more detailed discussions on diffusion mechanisms and the diffusion equations. Even though this chapter may seem unnecessary it is important to understand diffusion before segregation is discussed in chapter 3.

2.2 Diffusion Mechanisms

In even absolutely pure materials atoms move from one lattice position to another, this process is known as self-diffusion. This can be detected by using radioactive tracers.

The movement of atoms can be influenced by factors like the size of the diffusing atom and the defects in the bulk. In the following section a few different diffusion mechanisms are discussed.

2.2.1 Vacancy diffusion

Vacancy diffusion takes place when an atom gains enough energy to move from its lattice position to a vacancy in close proximity (see figure 2.1). The number of vacancies helps to determine the extend of both self-diffusion and diffusion of substitutional atoms. The number of vacancies can be determent as follows

$$N_V = N_0 \exp\left(\frac{E_V}{RT}\right) \qquad (2.1)$$

with N_0 the number lattice positions, E_V the vacancy formation energy, R the universal gas constant and T the temperature [18]. Examples of vacancy and self-diffusion are tabulated in table 2.1.

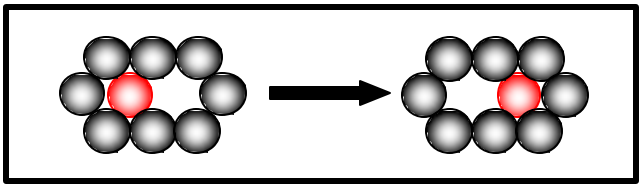

Figure 2.1: Illustration of vacancy diffusion [18].

Diffusion Couple	**Q ($kJ.mol^{-1}$)**	**D_0 ($m^2.s^{-1}$)**
Self-diffusion [18]		
Fe in FCC Fe	279.2	6.5×10^{-5}
Cu in FCC Cu	206.4	3.6×10^{-5}
Al in FCC Al	134.8	1.0×10^{-5}
Vacancy diffusion [18]		
Ni in Cu	242.2	2.3×10^{-4}
Cu in Ni	257.5	6.6×10^{-5}
Zn in Cu	188.8	7.8×10^{-5}

Table 2.1: Diffusion coefficients for vacancy and self-diffusion, where Q is the activation energy and D_0 the standard activation energy.

2.2.2 Interstitial diffusion

Interstitial diffusion occurs when a small interstitial atom gains enough energy to move from an interstitial site to another vacant interstitial site (see figure 2.2). This as the name states is limited to interstitial atoms. Examples of vacancy and self-diffusion are tabulated in table 2.2.

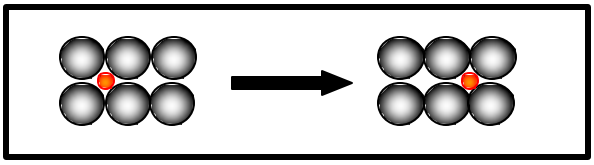

Figure 2.2: Illustration of interstitial diffusion [18].

Diffusion Couple	**Q ($kJ.mol^{-1}$)**	**D_0 ($m^2.s^{-1}$)**
Interstitial diffusion [18]		
C in FCC Fe	137.7	2.3×10^{-5}
N in FCC Fe	144.9	3.4×10^{-7}
H in FCC Fe	43.1	6.3×10^{-7}

Table 2.2: Diffusion coefficients for interstitial diffusion.

2.2.3 Ring diffusion

Ring exchange was postulated in the 1950s, as the most important mechanism for diffusion in solid-solution alloys (see figure 2.3) [17]. The deformation or distortion of the lattice is comparable to that of interstitial mechanism for solvent atoms. The energy required for this to take place is rather high, thus the probability for it to take place is low.

Ring diffusion is still considered a feasible mechanism for substitutional diffusion in some “open” crystal structures, such as diamond cubic, body centred cubic and rhombohedral [17].

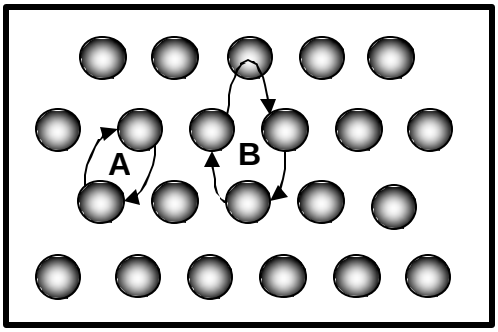

Figure 2.3: Illustration of ring diffusion; A – Direct exchange, B – Cyclic exchange [17].

2.3 Activation Energy

In order for atoms to move from one lattice position to the other lattice position, the diffusing and surrounding atoms must deform, for the diffusing atom to move past the surrounding atoms. In order for this to happen, enough energy must be supplied to the atom to move it to the new position, as illustrated in figure 2.3. The atom is in a low energy position in the beginning, for it to move to a new position it must overcome an energy barrier. This energy barrier is known as the activation energy Q.

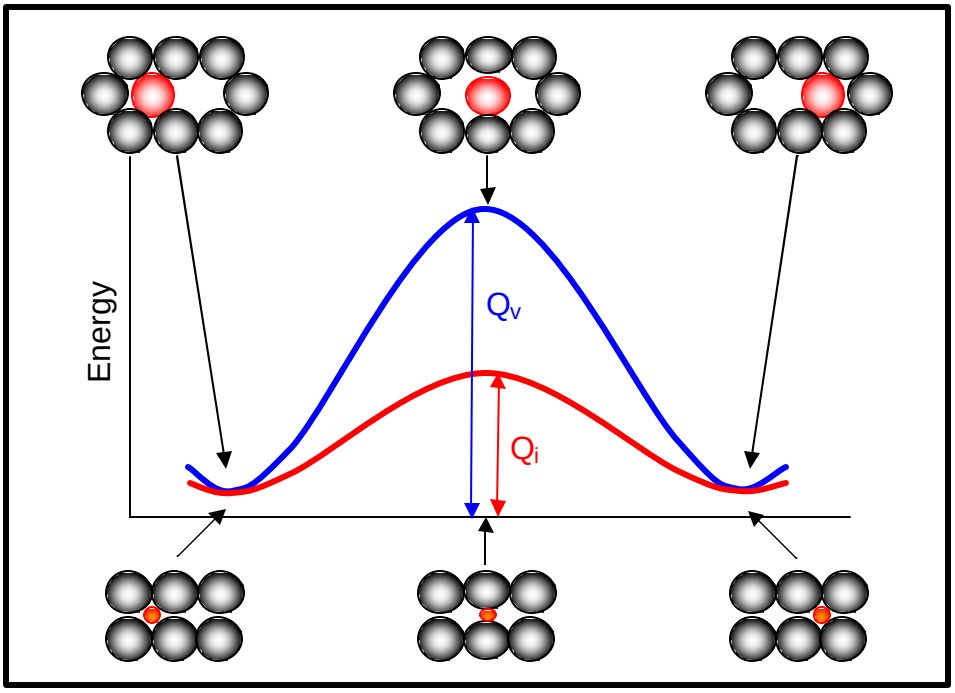

Figure 2.4: Illustration of the energy needed, activation energy, for vacancy and interstitial diffusion [18].

Normally less energy is required for interstitial atoms to move past the surrounding atoms. Thus the activation energy for interstitial diffusion Q_i is lower than for vacancy diffusion Q_v.

2.4 Diffusion Equations

2.4.1 Rate of diffusion (Fick's first law)

The flux J of atoms that flows from a high concentration area to a low energy area, is defined as the number of atoms passing through a plane of a unit area in a unit time, as illustrated in figure 2.5.

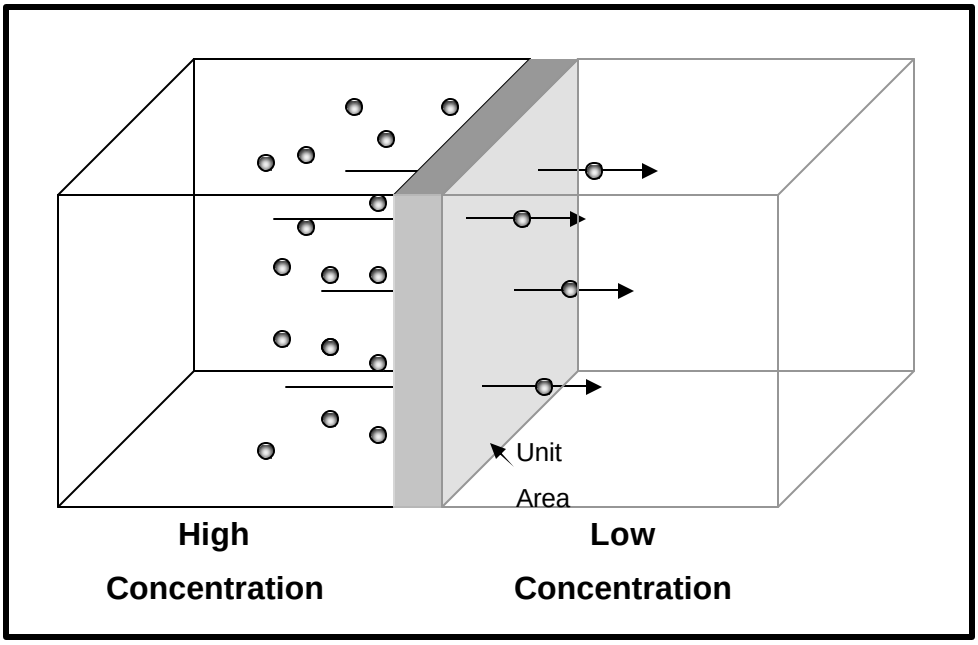

Figure 2.5: The flux of atoms that flows through a plane from a high to a low concentration area [19].

Fick's first law explains that the net flux of atoms is [17]

$$J = -D\frac{\Delta c}{\Delta x} \qquad (2.2)$$

Where J is the flux, D is the diffusivity or diffusion coefficient and Dc/Dx is the concentration gradient.

2.4.2 Temperature and the diffusion coefficient

It is clear that the temperature plays a fundamental part in diffusion. The relationship between the diffusion coefficient and the temperature is given by the Arrhenius equation [17]

$$D = D_0 \exp\left(\frac{-Q}{RT}\right) \tag{2.3}$$

with D_0 the standard diffusion coefficient, Q the activation energy, R the gas constant and T the temperature.

If the temperature increases the diffusion coefficient will increase, as well as the flux of atoms. At low temperatures, usually below about 0.4 times the absolute melting temperature of the material, the diffusion rate is very low and may not be significant [19].

2.4.3 Composition profile (Fick's second law)

Fick's second law describes the diffusion of atoms. One solution for the differential equation

$$\frac{dc}{dt} = D\left(\frac{d^2c}{dx^2}\right) \tag{2.4}$$

whose solution depends on the boundary conditions is

$$\frac{c_s - c_x}{c_x - c_0} = erf\left(\frac{x}{2\sqrt{Dt}}\right) \tag{2.5}$$

where c_s the concentration of the diffusing atoms at the surface, c_0 the initial concentration of the diffusing atom in the material, c_x the concentration of the diffusing atoms at a location x below the surface after a time t and D the diffusion coefficient [17].

Chapter 3

Segregation

3.1 Introduction

In the previous chapter diffusion, the movement of atoms was discussed. In this chapter a more in-depth discussion of the movement of atoms from the bulk to the surface is given. This is known as segregation.

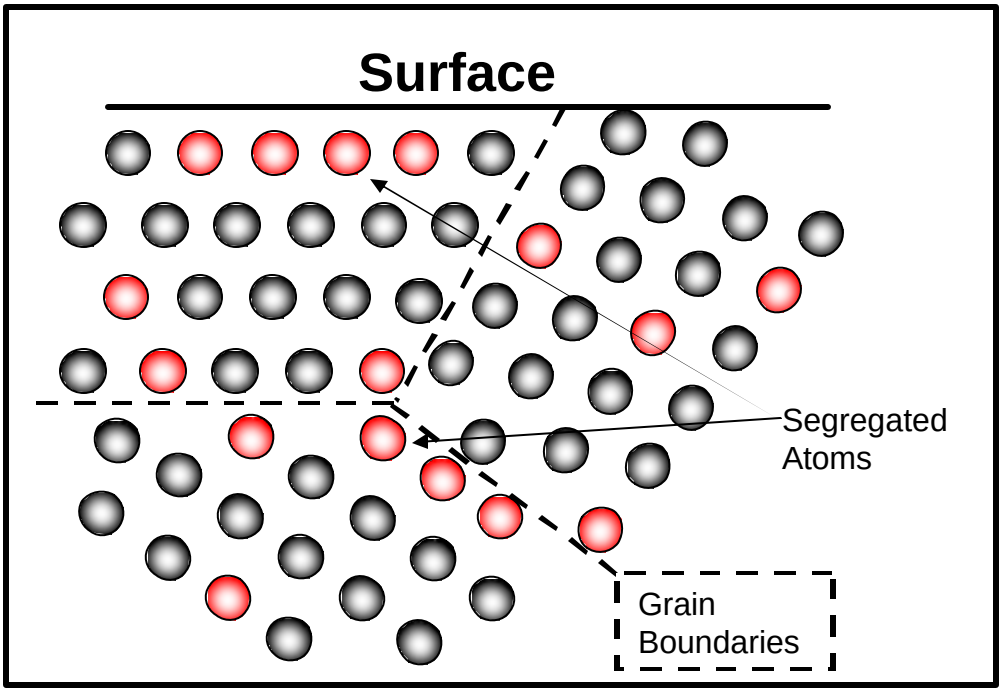

Figure 3.1: Diagram to illustrate the different types of segregation.

Segregation usually occurs in metal alloys during heating. When sufficient energy is supplied to an alloy, the alloying atoms will redistribute themselves in the material in such a way that the total energy of the system is minimized. In this redistribution some of the atoms move to the surface.

Even though segregation can be broken up in grain boundary segregation and surface segregation, as illustrated in figure 3.1, only the latter will be considered in the rest of the chapter.

3.2 Segregation Energy

When dealing with segregation theory it is often useful to divide the crystal into a series of N layers (with a thickness d) and treat the segregation as a layer by layer process in which the solute atoms diffuse from the bulk layers to the surface layers (see figure 3.2).

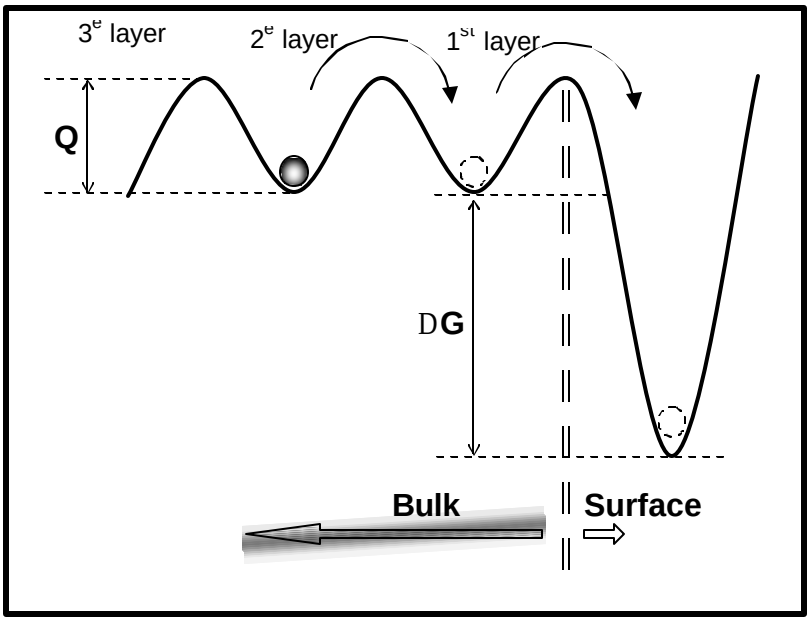

Figure 3.2: Illustration of the energies involved during segregation.

As mentioned before, the activation energy *Q* is the amount of energy necessary for an atom to move from one lattice position to another or as figure 3.2 suggests, from one low energy position to the next. When an atom diffuses from the first bulk layer to the surface, it experiences an additional potential *DG*. As a result this atom must receive energy of at least *Q+DG* in order to diffuse back into the bulk, from the surface. This energy, *DG* is known as the segregation energy. The atom that eventually remains on the surface as time increases, at a particular temperature, depends largely on the "depth" of the potential, *DG*, on the surface.

3.3 Segregation Equilibrium

In chapter 3.1, segregation is defined as the movement from the bulk to the surface of a crystal, to minimize the total energy of the system. To avoid any

confusion the definition is expanded further to include the following assumptions [13]:

1. The crystal is regarded as a closed system consisting of two phases, the surface and the bulk and both these phases are open systems.
2. The surface is finite and the bulk infinite in size.
3. Atoms may be exchanged between the two phases until the energy of the system is minimized.

Lupis [17] derived an equation for equilibrium conditions for a closed system with p-phases

$$dG = \sum_{n=1}^{p}\left[\sum_{i=1}^{m}\left(n_i^n\, d\mu_i^n\right) + \sum_{i=1}^{m}\left(d n_i^n\, \mu_i^n\right)\right] \qquad (3.1)$$

where n is the phase, n_i^n the number of moles of type i in phase n and μ_i^n the chemical potential of type i in phase n.

By using equation 3.1, an equation can be derived for the equilibrium conditions of atoms segregating to the surface. In equilibrium conditions we have two phases; the bulk (B) phase that is infinite and the surface (ϕ) phase that is finite. Assume that the number of atoms that occupy the surface is finite and stays constant. Thus n^f = constant. If the atoms can move freely between the two phases equation 3.1 becomes [20]

$$dG = \left[\sum_{i=1}^{m}\left(n_i^f\, d\mu_i^f\right) + \sum_{i=1}^{m}\left(n_i^B d\mu_i^B\right)\right] + \left[\sum_{i=1}^{m}\left(d n_i^f\, \mu_i^f\right) + \sum_{i=1}^{m}\left(d n_i^B\, \mu_i^B\right)\right] \qquad (3.2)$$

where n_i^f is the amount of atoms of type *i* on the surface, μ_i^f the chemical potential of type *i* on the surface, n_i^B the amount of atoms of specie *i* in the bulk and μ_i^B the chemical potential of specie *i* in the bulk.

The Gibbs-Duhem expression states that $\sum_i \left(n_i^f d\mu_i^f \right)$ is null [20]. Thus eq. (3.2) reduces to:

$$dG = \sum_{i=1}^{m} \left(dn_i^f \mu_i^f \right) + \sum_{i=1}^{m} \left(dn_i^B \mu_i^B \right) \tag{3.3}$$

Since the surface phase is finite, it can be written that

$$\sum_{i=1}^{m} n_i^f = n^f \tag{3.4}$$

Due to the fact that the number of atoms on the surface stays constant, the number of atoms that jumps on to the surface is equal to the number of atoms leaving the surface. Thus

$$dn_1^f + dn_2^f + \ldots + dn_m^f = 0 \tag{3.5}$$

Eq. (3.5) can also be written as

$$-dn_m^f = dn_1^f + dn_2^f + \ldots + dn_{m-1}^f \tag{3.6}$$

By inserting eq. (3.6) into eq. (3.3) the change in Gibbs free energy is obtained

$$\left[\sum_{i=1}^{m-1} \left(\mu_i^f - \mu_i^B - \mu_m^f + \mu_m^B \right) dn_i^f \right] \geq 0 \tag{3.7}$$

This only holds true if [13]

$$m_i^f - m_i^B - m_m^f + m_m^B = 0 \tag{3.8}$$

Eq. (3.8) is the equilibrium condition for atoms segregating from the bulk of the material to the surface.

3.3.1 Langmuir-McLean equation

If a binary alloy is considered with the solvent matrix represented by a two $(m=2)$ and the solute represented by a one $(i=1)$, eq. (3.8) becomes

$$m_1^f - m_1^B - m_2^f + m_2^B = 0 \tag{3.9}$$

According to the regular solution model [14] the chemical potential for a binary alloy can be written as

$$\begin{aligned} m_1^n &= m_1^{0,n} + \Omega_{12}\left(X_2^n\right)^2 + RT\ln\left(X_1^n\right) \\ m_2^n &= m_2^{0,n} + \Omega_{12}\left(X_1^n\right)^2 + RT\ln\left(X_2^n\right) \end{aligned} \tag{3.10}$$

with m_1^n represents the chemical potential of element 1 in phase n, $m_1^{0,n}$ the standard chemical potential of element 1 in phase n, m_2^n the chemical potential of element 2 in phase n, $m_2^{0,n}$ the standard chemical potential of element 2 in phase n, X_1 the concentration of element 1, X_2 the concentration of element 2 and Ω_{12} the chemical interaction parameter between element 1 and 2.

Eq. (3.10) can then be expanded to four equations that include both the surface and the bulk phase

$$\begin{aligned} m_1^f &= m_1^{0,f} + \Omega_{12}\left(X_2^f\right)^2 + RT\ln\left(X_1^f\right) \\ m_2^f &= m_2^{0,f} + \Omega_{12}\left(X_1^f\right)^2 + RT\ln\left(X_2^f\right) \\ m_1^B &= m_1^{0,B} + \Omega_{12}\left(X_2^B\right)^2 + RT\ln\left(X_1^B\right) \\ m_2^B &= m_2^{0,B} + \Omega_{12}\left(X_1^B\right)^2 + RT\ln\left(X_2^B\right) \end{aligned} \tag{3.11}$$

By inserting eq (3.11) into eq (3.9) and rearranging, the Bragg-Williams equation is obtained [14]:

$$\frac{X_1^f}{1-X_1^f} = \frac{X_1^B}{1-X_1^B}\exp\left(\frac{\Delta G + 2\Omega_{12}\left(X_1^f - X_1^B\right)}{RT}\right) \tag{3.12}$$

with X_1^f the surface concentration of element 1, X_1^B the bulk concentration of element 1, $\Delta G = m_1^{0,B} - m_1^{0,f} - m_2^{0,B} + m_2^{0,f}$ the standard segregation energy and Ω_{12} the chemical interaction parameter between element 1 and 2.

By taking the interaction parameter as null, the Bragg-Williams equation reduce to the Langmuir-McLean equation

$$\frac{X_1^f}{1-X_1^f} = \frac{X_1^B}{1-X_1^B}\exp\left(\frac{\Delta G}{RT}\right) \tag{3.13}$$

Figure 3.3 shows the equilibrium concentration calculated by eq. (3.13).

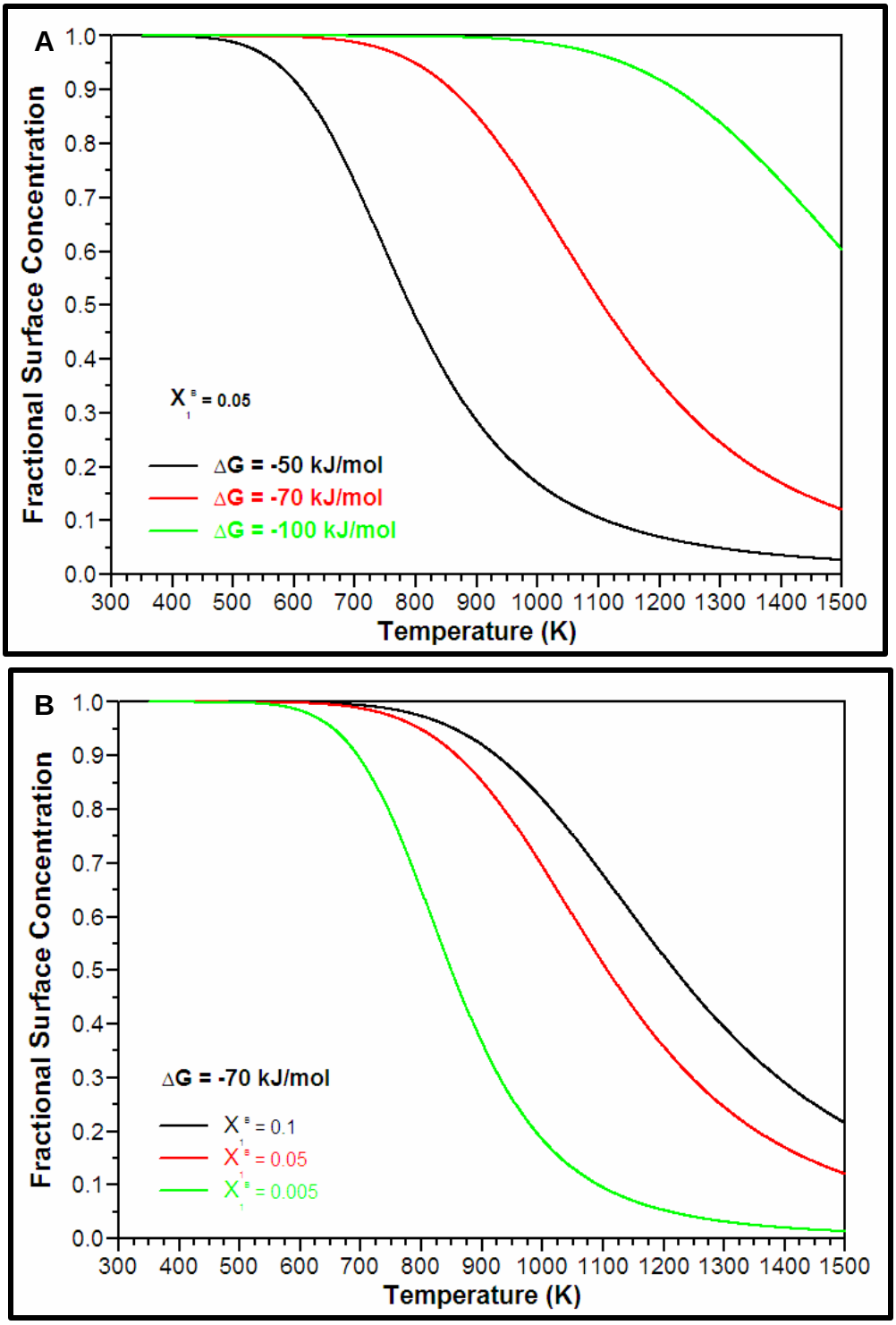

Figure 3.3: Shows the equilibrium concentration on the surface. In figure A the segregation energy, DG, is changed and in figure B the bulk concentration is changed [22].

3.4 Kinetics of Surface Segregation

3.4.1 Semi-infinite solution of Fick's equations

The purpose of this section is to provide a solution to Fick's first law, as it is often used to describe the kinetic part of segregation.

Consider a crystal with a uniform bulk concentration. If the atoms segregating into the surface layer have no interaction with one another, the rate of segregation is independent of the surface concentration.

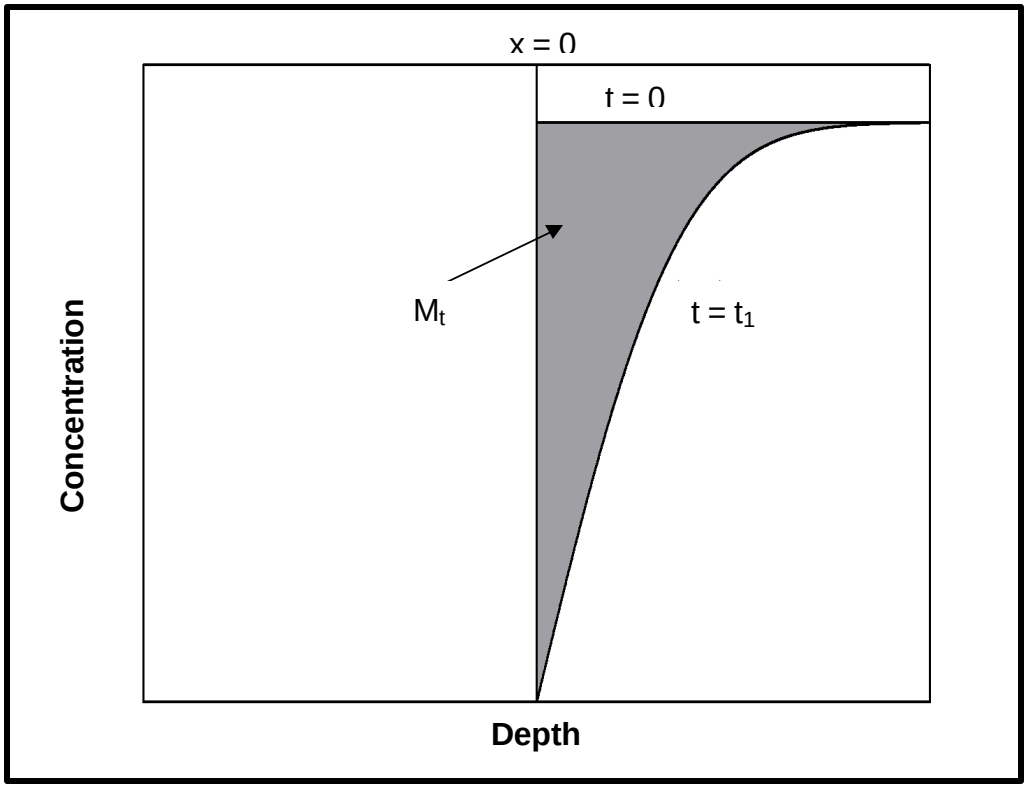

Figure 3.4: Boundary conditions used to solve Fick's first law.

In Figure 3.4 two boundary conditions are shown that are of importance in this derivation [21]:

$$C^x = 0 \qquad \text{for} \qquad x = 0 \qquad \text{and} \qquad t \geq 0\,,$$

and assuming that the bulk concentration of the segregating atoms is uniform,

$$C^x = C^B \qquad \text{for} \qquad x > 0 \qquad \text{and} \qquad t = 0\,.$$

Using the above boundary conditions to solve Fick's first law [20], it is possible to find an expression for the bulk concentration [20,21,22]:

$$C^x = C^B \operatorname{erf}\left(\frac{x}{2\sqrt{Dt}}\right) \tag{3.13}$$

where C^x represents the bulk concentration at position x after a time t, C^B represents the initial bulk concentration and D is the diffusion coefficient.

Using eq. (3.13), the flux can then be written as [21]

$$J_{x=0} = \left(D\frac{\partial C}{\partial x}\right)_{x=0} = \frac{DC^B}{\sqrt{pDt}}\,. \tag{3.14}$$

By integrating eq. (3.14) it is possible to obtain the number of atoms (M_t) that pass through a surface A at $x = 0$ in a given time t [20,22]:

$$\begin{aligned} M_t &= A\int_{t=0}^{t} J\,dt \\ &= 2AC^B\left(\frac{Dt}{p}\right)^{\frac{1}{2}}. \end{aligned} \tag{3.15}$$

The atoms moving through *A* is assumed to remain in the surface layer, the concentration of the segregating atoms in the surface can be determined by dividing eq. (3.15) by the volume of the surface layer:

$$C^f = \frac{2AC^B\left(\frac{Dt}{p}\right)^{\frac{1}{2}}}{Ad} = \frac{2}{d}C^B\left(\frac{Dt}{p}\right)^{\frac{1}{2}} \tag{3.16}$$

where C^f is the surface concentration, C^B is the bulk concentration and *d* is the thickness of the layer [22]. Since the initial concentration of the crystal is uniform, the concentration of segregating elements in the surface layer is the same as the bulk concentration; the initial bulk concentration is therefore added to eq. (3.16), which leads to [20,21,22,23]

$$C^f = C^B\left(1+\frac{2}{d}\left(\frac{Dt}{p}\right)^{\frac{1}{2}}\right). \tag{3.17}$$

Eq. (3.17) is often used to calculate the surface concentration during segregation.

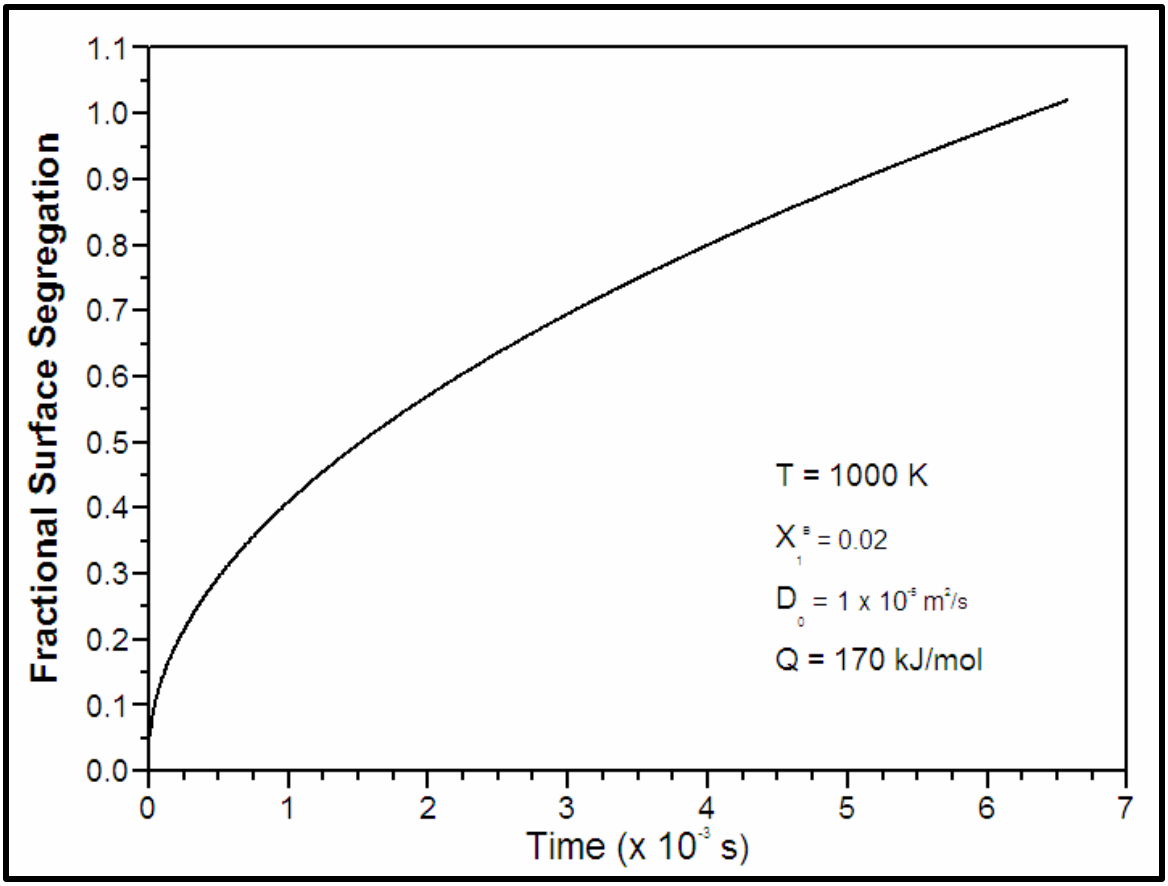

Figure 3.5: The change in the surface concentration with time is shown. The equilibrium surface concentration is not brought into consideration by this model.

In figure 3.5 a typical surface concentration profile generated with eq. (3.17) is shown. It is clear that this solution of Fick's first law predicts that the surface concentration will increase to infinity as time increases to infinity and therefore it cannot predict the equilibrium condition as observed experimentally in surface segregation [24]. However the Fick model can predict the segregation for short time intervals. The next section describes the modified Darken model that describes the kinetic and equilibrium conditions of a segregation profile.

3.4.2 The modified Darken approach

The basic Darken model proposes that the flux of species *i* through a plane at *x* = *b* is given by [20,22]

$$J_i = -M_i C_i^{(b)} \left(\frac{\partial m_i}{\partial x} \right)_{x=b} \tag{3.18}$$

where m_i is the chemical potential of species *i*, $C_i^{(b)}$ is the concentration of species *i* in the plane and M_i is the mobility of species *i*. The main difference between Fick's model described in the previous section and the Darken model is that the process that drives diffusion. The Fick model assumes that the driving force is the concentration gradient while the Darken model assumes that the chemical potential gradient is the driving force. This means that the Darken model relies on the minimization of energy as the driving force behind diffusion.

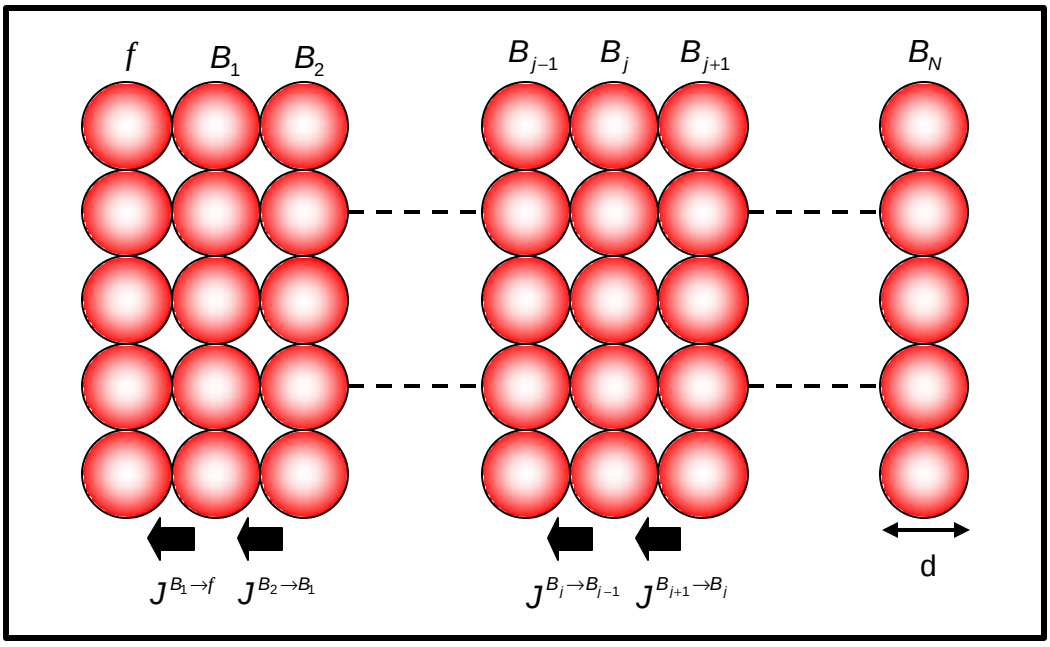

Figure 3.6: Representation of the atomic flux as proposed for the modified Darken model [24].

The modified Darken model proposed by Du Plessis [20] defines a crystal as a system of discrete layers parallel to the surface layer, as shown in Figure 3.6. Du Plessis also rewrote the term $\frac{\partial m_i}{\partial x}$ in a discrete form:

$$-\frac{\partial m_i}{\partial x} = \frac{\Delta m_i^{(j+1\to j)}}{d}$$

with d the thickness of the layers. The change in the chemical potential was also rewritten as

$$\Delta m_i^{(j+1\to j)} = \left(m_i^{(j+1)} - m_i^{(j)}\right) - \left(m_m^{(j+1)} - m_m^{(j)}\right), \qquad (3.20)$$

where $m_i^{(j+1)}$ is the chemical potential of species i in layer j+1, $m_i^{(j)}$ is the chemical potential of species i in layer (j), $m_m^{(j+1)}$ is the chemical potential of species m in layer j+1 and $m_m^{(j)}$ is the chemical potential of species m in layer j.

If atoms move from layer j+1 to layer j, the flux of atoms (eq. (3.18)) can be written as [13,22]

$$J_i^{(j+1\to j)} = -M_i C_i^{(j+1)} \frac{\Delta m_i^{(j+1\to j)}}{d}. \qquad (3.21)$$

A similar equation can be obtained for atoms moving from layer j to j+1:

$$J_i^{(j\to j+1)} = -M_i C_i^{(j)} \frac{\Delta m_i^{(j+1\to j)}}{d}. \qquad (3.22)$$

Since the driving force behind segregation is the minimization of the Gibbs free energy, the change in the chemical potential will determine which one of eq. (3.21) or (3.22) is used in calculating the flux $J_i^{(j\to j+1)}$. If $\Delta m_i^{(j+1\to j)} > 0$, the Gibbs free energy will decrease when atoms move from layer *j*+1 to *j*, and eq.(3.21) is used in the calculations. If $\Delta m_i^{(j+1\to j)} < 0$, the Gibbs free energy will decrease when atoms move from layer *j* to *j*+1, and eq. (3.22) is used in the calculations.

The rate at which the concentration in layer *j* is changing can be calculated with equations (3.21) and (3.22) [20,22]:

$$\frac{\partial C_i^{(j)}}{\partial t} = \frac{\left(J_i^{(j+1\to j)} - J_i^{(j\to j-1)}\right)}{d}. \tag{3.23}$$

Expanding eq. (3.23) in terms of a system of $(m-1)(N+1)$ equations enables the calculation of the rate at which species concentration changes in layers [22]:

$$\begin{aligned}
\frac{\partial X_i^{(f)}}{\partial t} &= \left(\frac{M_i^{(B_1\to f)} X_i^{(B_1)}}{d^2}\Delta m_i^{(B_1\to f)}\right) \\
\frac{\partial X_i^{(B_1)}}{\partial t} &= \left(\frac{M_i^{(B)} X_i^{(B_2)}}{d^2}\Delta m_i^{(B_2\to B_1)} - \frac{M_i^{(B_1\to f)} X_i^{(B_1)}}{d^2}\Delta m_i^{(B_1\to f)}\right) \\
&\vdots \\
\frac{\partial X_i^{(j)}}{\partial t} &= \left(\frac{M_i^{(B)} X_i^{(j+1)}}{d^2}\Delta m_i^{(j+1\to j)} - \frac{M_i^{(B)} X_i^{(j)}}{d^2}\Delta m_i^{(j\to j-1)}\right). \\
&\vdots
\end{aligned} \tag{3.24}$$

The system of differential equations can be solved numerically, enabling the calculation of the concentration of species *i* in any layer as a function of time. In studies involving ideal binary alloys, the above rate equations are often rewritten with the aid of eq. (3.11) and eq. (3.8) to allow binary alloy specific calculations:

$$
\begin{aligned}
\frac{\partial X_1^{(f)}}{\partial t} &= \left(\frac{M_1^{(B_1 \to f)} X_1^{(B_1)}}{d^2}\right)\left[\Delta G + RT \ln\left(\frac{X_1^{(B_1)} X_2^{(f)}}{X_1^{(f)} X_2^{(B_1)}}\right)\right] \\
\frac{\partial X_1^{(B_1)}}{\partial t} &= \left(\frac{M_1^{(B)} X_1^{(B_2)}}{d^2}\right)\left[RT \ln\left(\frac{X_1^{(B_2)} X_2^{(B_1)}}{X_1^{(B_1)} X_2^{(B_2)}}\right) - RT \ln\left(\frac{X_1^{(B_1)} X_2^{(f)}}{X_1^{(f)} X_2^{(B_1)}}\right)\right] \\
&\vdots \\
\frac{\partial X_1^{(B_j)}}{\partial t} &= \left(\frac{M_1^{(B)} X_1^{(B_{j+1})}}{d^2}\right)\left[RT \ln\left(\frac{X_1^{(B_{j+1})} X_2^{(B_j)}}{X_1^{(B_j)} X_2^{(B_{j+1})}}\right) - RT \ln\left(\frac{X_1^{(B_j)} X_2^{(B_{j-1})}}{X_1^{(B_{j-1})} X_2^{(B_j)}}\right)\right] \\
&\vdots
\end{aligned}
\tag{3.25}
$$

The above rate equations is capable of simulating both the kinetic and equilibrium conditions associated with segregation, as indicated in figure 3.7 [22,24].

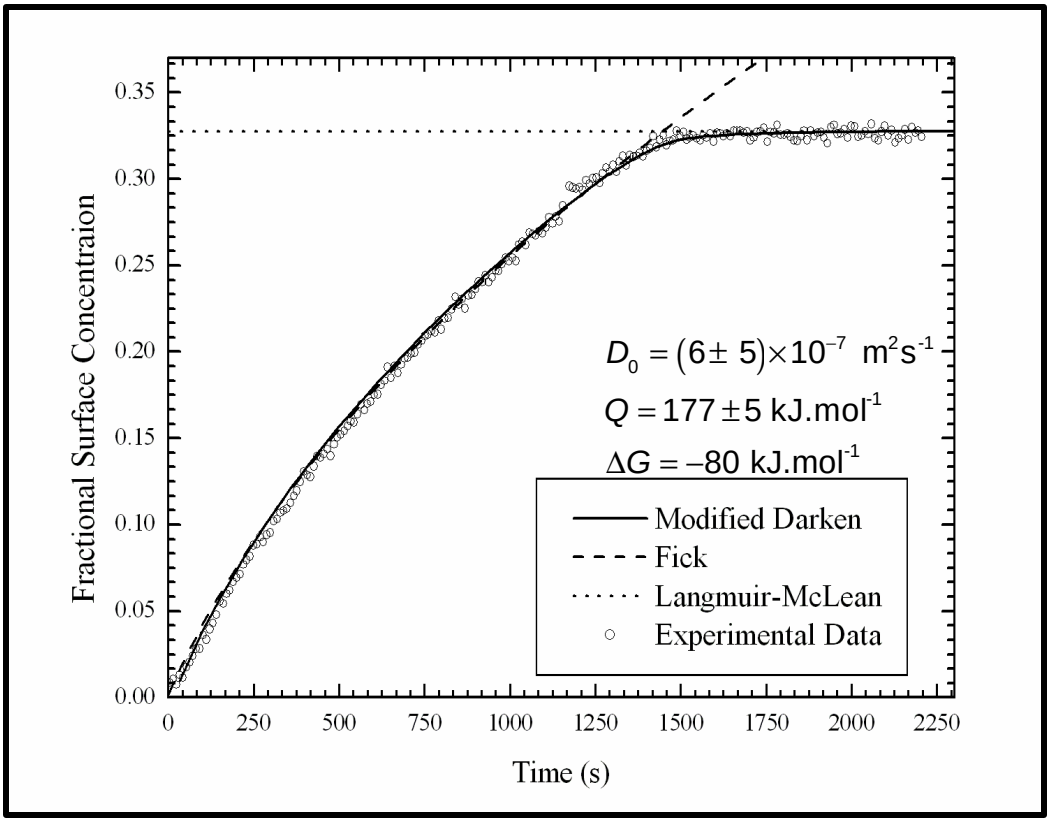

Figure 4.5: The figure shows a comparison of the surface segregation as calculated with Fick's model and the modified Darken model [25].

The kinetic part of segregation is similar for both Fick's model and Modified Darken model. Fick's model is unable to describe the equilibrium surface concentration, while the modified Darken follows the experimental data closely.

An experimental segregation study was conducted by Erasmus, et. al. [25]. This study focused on the segregation of Sb from Cu crystals and a typical result from the study is shown in Figure 4.5. The dashed line represents the Fick's theoretical fit model. The Fick model accurately describes the kinetics of segregation from time t = 0 s to time t = 1100 s. The model however cannot describe the equilibrium condition seen from the experimental data and predicted by the Langmuir-McLean equation. The solid line is the theoretical fit of the experimental data obtained from the modified Darken model. This model accurately describes both the conditions associated with segregation and the equilibrium value obtained from the fit also matches the value predicted by the Langmuir-McLean equation. The modified Darken model is used in collaboration with the oxidation theory in the next chapter to derive a new model to describe the results obtained in this study. See derivation in results and discussion.

Chapter 4

Oxidation

4.1 Introduction

Oxidation can be defined as the process of combining oxygen with some other substance or a chemical change in which an atom loses electrons [26]. In this study the focus is on the reaction between a metal and oxygen.

The exposure of almost any metal to gaseous oxygen can cause the formation of an oxide. The formed oxide is not always seen as negative. The oxide constitutes a protective layer which separates the metal from the gaseous oxygen. Oxides is only one type of protective layers on metals, other include protective layers such as sulphides and halides.

4.2 Growth of Oxide Layers

The formation of an oxide layer may be broken up in four basic stages [27] and is illustrated in figure 4.1:

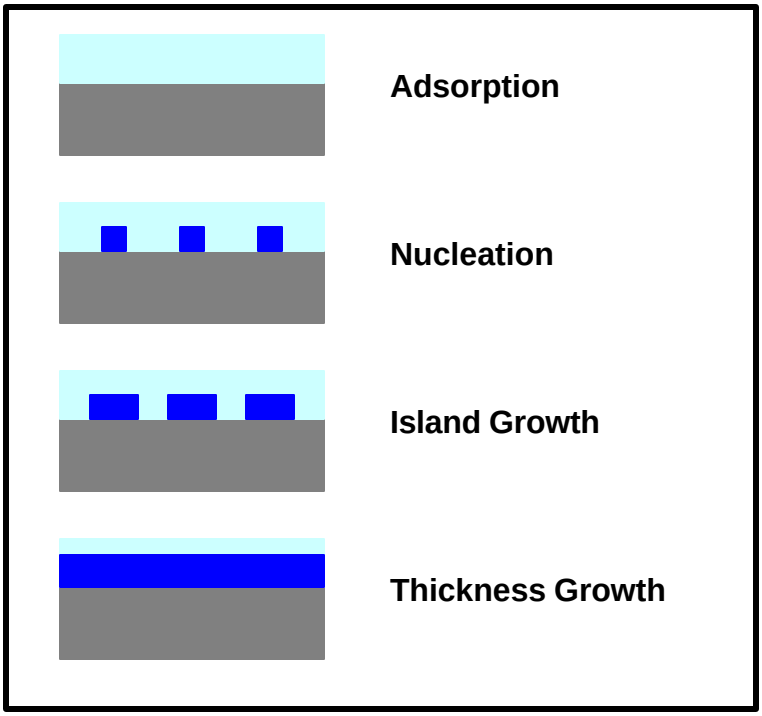

Figure 4.1: A schematic illustration of the four stages during oxidation.

- A relatively fast physisorption of the oxygen molecules on the substrate surface.
- The dissociation of the molecules which is followed by chemisorption. The reactivity of the oxygen decrease, with the saturation and nucleation of the oxygen on the surface.
- The nuclei grow laterally with a constant stable increase of oxygen.
- As soon as the surface is completely covered with an oxide layer, the thickness will increase slowly. The change in thickness is usually logarithmic or parabolic, depending on the substrates properties.

The distinction of the stages is only visible in metals with low reactivity, while metals with a high reactivity the distinction between the first three stages is not clear [32].

4.2.1 Adsorption

Adsorption is the first step of oxidation. Adsorption is the formation of a layer of gas, liquid or solid on the surface of a solid or, less frequently, of a liquid [33]. In the most cases of oxidation, the adsorption takes place in two steps, first physisorption takes place and then after the dissociation of the oxygen chemisorption takes place. Figure 4.2 is an illustration of the difference in bonding of the adsorbate.

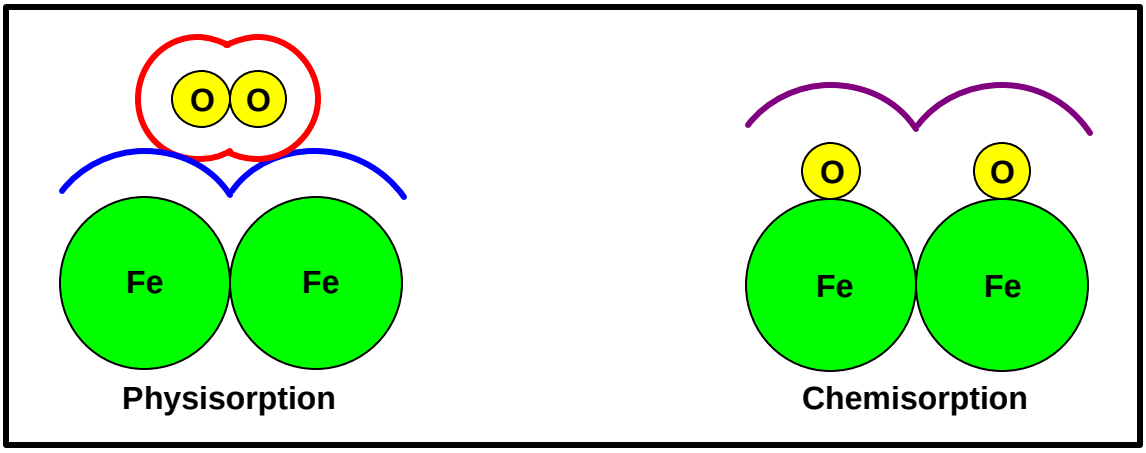

Figure 4.2: Schematic illustration for the different types of adsorption.

4.2.1.1 Physisorption

The weakest form of adsorption to a solid surface is known as physical adsorption, or physisorption [28]. It is characterized by the lack of a chemical bond, there exists an attractive force between the absorbate and the surface.

One possibility is that there it is a van der Waals interaction between the gas molecule and the solid surface.

4.2.1.2 Chemisorption

In the beginning of the previous century, scientists generally believed that all the adsorption that takes place were physisorption. The absorbed layers were viewed as compressed layers of vapour, with little or no interaction with the substrate [28]. Experimental evidence soon accumulated that pointed to a distinctly different form of adsorption.

Langmuir (1916) introduced and extensively investigated the idea that there can exist a strong short range forces between adsorbates and a substrate [29]. The surface was viewed as a Chinese checkerboard that defines the density of potential absorption sites. When a gas atom hits the surface it can either bounce of the surface or it can form a surface chemical bond, the latter is called chemisorption.

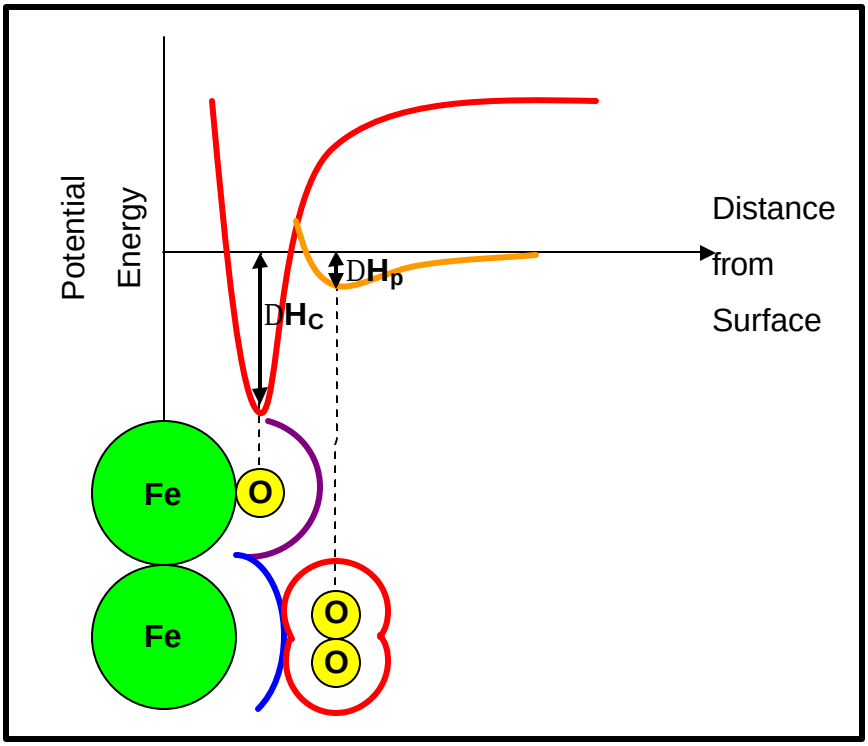

Figure 4.3: The potential energy curves of the absorbate, based on Ni-H work done by G.C. Bond [30].

To explain the difference between physisorption and chemisorption, it can easily be shown by the potential energy curves of the absorbate, illustrated in figure 4.3. As a gas molecule approaches the surface, an attractive force will start to form and will cause a decrease in the potential energy. At the lowest point on this potential energy curve physisorption will take place. A repulsive force will develop if distance between the species decrease more. The heat of physisorption is illustrated as ΔH_p. For chemisorption the oxygen molecule must first dissociate into atoms, before a chemical bond can form and with a chemical bond the distance between the atoms is much smaller, thus the potential energy for chemisorption (ΔH_c) is larger.

4.2.2 Nucleation

When a reaction leads to the formation of a new phase in a system, this new phase often appears as a small nucleus in the old phase [31]. The precipitate nucleates most easily at grain boundaries or other lattice defects [31]. The microscopic roughness of the metal surface and the extended defect regions such as stacking faults and dislocations in the metal may sometimes play an important roles as preferred sites at which elemental stable nuclei can form [30]. Consider the classical nucleation of spherical nucleus, to calculate the rate of nucleation [32].

For the formation of a sphere with radius r, the change in free energy is given as:

$$\Delta G = 4\pi r^2 s + \frac{4}{3}\pi r^3 \Delta G_v \qquad (4.1)$$

where s is the specific interfacial energy and ΔG_v is the free energy change per unit volume of particles formed during the reaction. The first term is the surface free energy and the second term is the volume free energy. ΔG is plotted as a function of r in figure 4.4. Nuclei with radii larger than r^* will tend to grow spontaneously. For nuclei with a radii smaller than r^*, the change in ΔG favours the disappearance rather than the growth of the nuclei [30]. At r^*:

$$\frac{d\Delta G}{dr} = 8\pi r^* s + 4\pi r^{*2} \Delta G_v = 0 \qquad (4.2)$$

which may be solved for r^* as:

$$r^* = \frac{-2s}{\Delta G_v} \qquad (4.3)$$

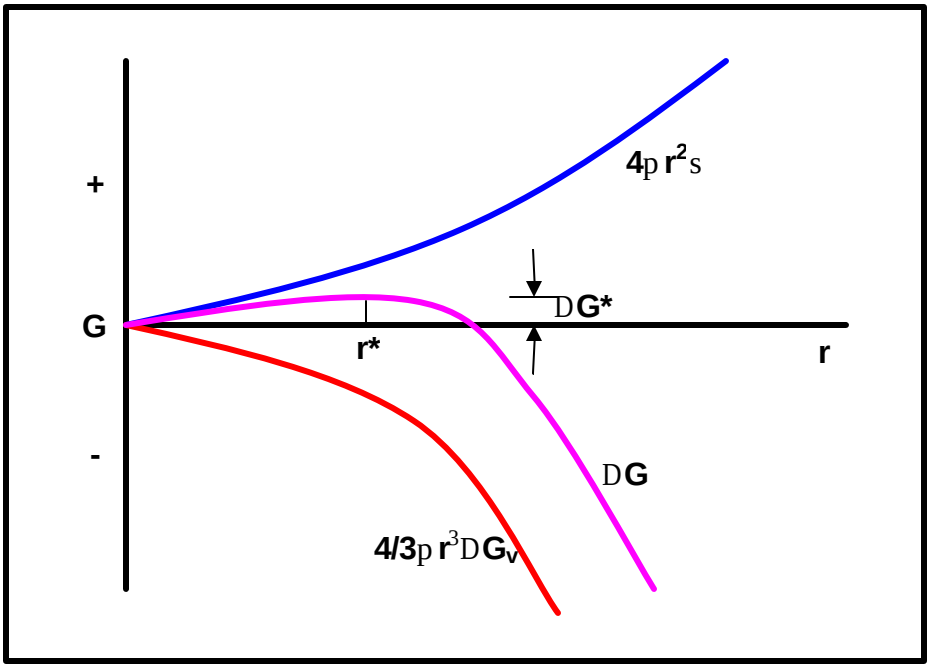

Figure 4.4: A schematic plot of the free energy versus the radius of a nucleating particle [30,31 and 33].

It is the value (DG_v), with DG_v the free energy at r^*, which enter into the nucleation rate as calculated from absolute reaction theory

$$J = vC^* = vC_0 e^{-\Delta G^*/RT} \qquad (4.4)$$

thus

$$Nucleation\ Rate \propto \exp\left(-\Delta G^*/RT\right) \qquad (4.5)$$

4.2.3 Island growth

Growth of the precipitate normally occurs by long range diffusion and redistribution of atoms [33]. In most cases the controlling factor is the diffusion step. The growth rate of the new phase increase with the increase in temperature

and decrease with the decrease in temperature, due to slower diffusion at lower temperature. The growth rate follows an Arrhenius relationship:

$$Growth\ Rate \propto \exp(-Q/RT) \tag{4.6}$$

where Q is the activation energy for the reaction, R is the gas constant and T the temperature.

4.2.4 Thickness growth

Consider the following equation [33]:

$$M(s) + \tfrac{1}{2}O_2(g) = MO(s) \tag{4.7}$$

the reaction product MO will separate the two reactants, as illustrated in figure 4.5.

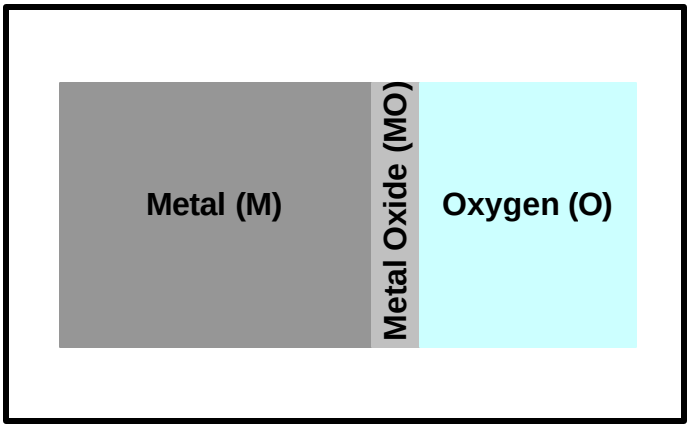

Figure 4.5: Schematic illustration of metal oxide formation.

Thus for the growth of the oxide layer, either the metal must be transported through the oxide layer to the oxide-oxygen interface or oxygen must be

transported to the oxide-metal interface or both. A more in depth discussion follow later in this chapter.

4.3 Oxidation Mechanisms

When Fe oxidises at high temperature it manifests into layers of FeO, Fe_3O_4 and Fe_2O_3 and thus provides an example of multi-layered systems. Due to the importance in society, the oxidation of Fe has been extensively investigated [34].

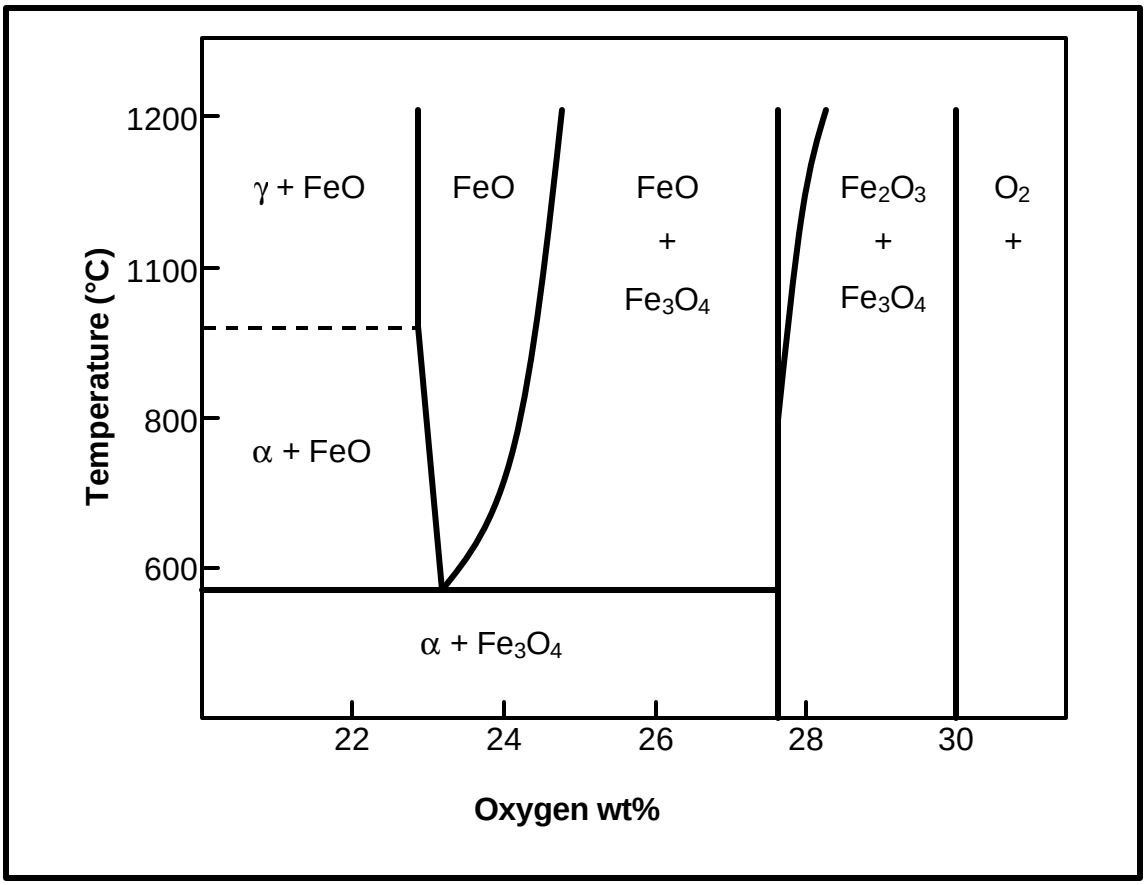

Figure 4.6: Phase diagram of iron-oxygen [32,34].

From the phase diagram it is clear that the wustite phase, FeO, does not form below 570°C, thus oxidation below this temperature will form layered scales of

Fe_2O_3 and Fe_3O_4, with Fe_3O_4 next to the metal. At temperatures higher than 570°C an extra layer of FeO will form, with FeO next to the metal.

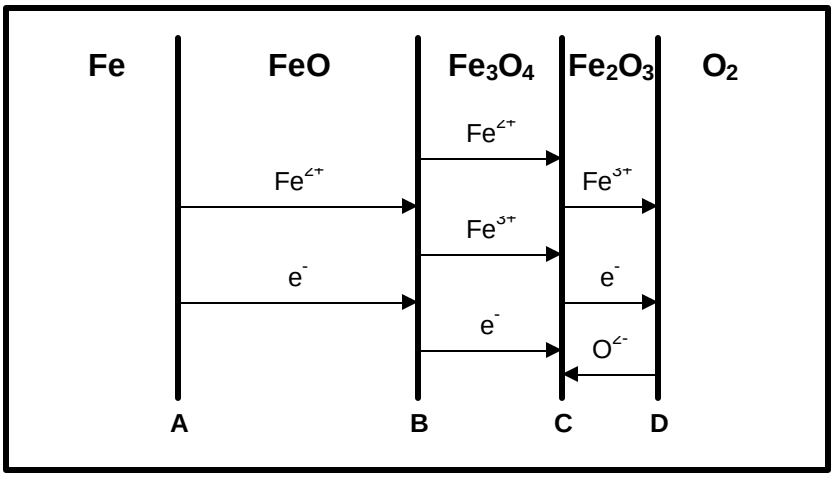

Figure 4.7: Oxidation mechanism of Fe to form a three-layered scale of FeO, Fe_3O_4 and Fe_2O_3 above 570°C [33].

A relative simple mechanism can be proposed to represent the oxidation of Fe as illustrated in figure 4.7. At the iron-wustite interface (Point A in fig 4.7), iron ionises according to

$$Fe = Fe^{2+} + 2e^{-} \tag{4.8}$$

The Fe ions and electrons migrate outward through the FeO (wustite) layer over vacancies and holes respectively. At the wustite-magnetite interface (Point B in fig 4.7), magnetite is reduced by the Fe ions and electrons according to

$$Fe^{2+} + 2e^{-} + Fe_3O_4 = 4FeO \tag{4.9}$$

The surplus Fe ions and electrons to this reaction migrate outwards through the magnetite layer, over the vacancies on the tetrahedral and octahedral sites and

over holes and excess electrons respectively. At the magnetite-haematite interface (Point C in fig 4.7), magnetite (Fe_3O_4) is formed according to

$$Fe^{n+} + ne^- + 4Fe_2O_3 = 3Fe_3O_4 \qquad (4.10)$$

The value for *n* is either 2 or 3 for the Fe^{2+} or Fe^{3+} ions respectively.

If the Fe ions are mobile in the haematite (Fe_2O_3) layer, they will migrate through this layer over the vacancies together with the electron and new haematite will form at the haematite-gas interface (Point D in fig 4.7) according to

$$2Fe^{3+} + 6e^- + \tfrac{3}{2}O_2 = Fe_2O_3 \qquad (4.11)$$

At this interface oxygen also ionise according to

$$\tfrac{1}{2}O_2 + 2e^- = O^{2-} \qquad (4.12)$$

If oxygen ions are mobile in the haematite layer, the Fe ions and electrons will react with oxygen ions diffusing inwards through the haematite layer over the vacancies forming new haematite at the magnetite-haematite interface according to

$$2Fe^{3+} + 3O^{2-} = Fe_2O_3 \qquad (4.13)$$

The corresponding electrons then migrate outwards through the haematite to take part in the ionisation of oxygen at the haematite-gas interface.

Due to the much greater mobility of defects in wustite, the wustite will be very thick compared with the magnetite and haematite layers. In fact, the relative thickness of $FeO:Fe_3O_4:Fe_2O_3$ are in the ration roughly 95:4:1 at 1000°C [33].

4.4 Rate of Oxidation

Oxidation can take place at three different rates.

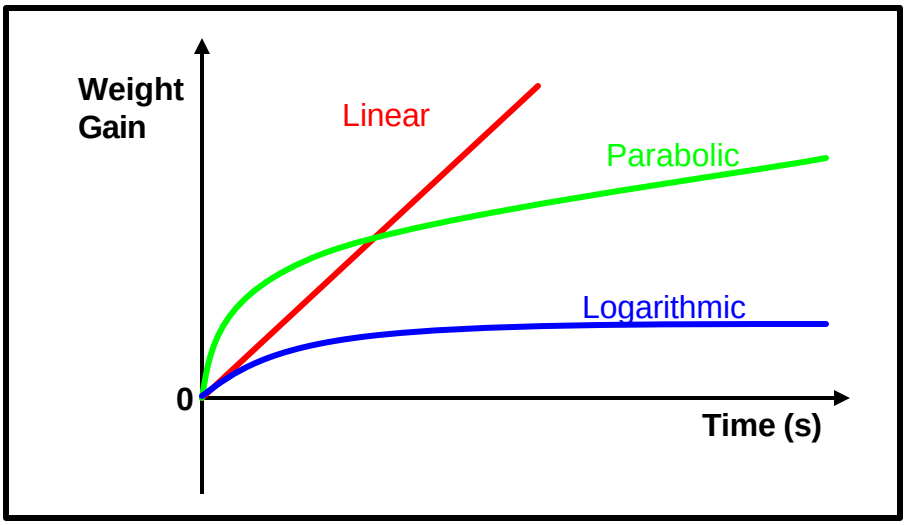

Figure 4.8: An illustration of the three oxidation rate laws.

4.4.1 Linear growth

Linear growth appears when the oxide is unable to hinder the access of the oxygen to the metals surface. This occurs when the oxide that is formed from the given volume of metal is too small to completely cover the surface of the metal. If the oxide cracks, a normally parabolic type of weight increase appears to be linear.

Linear growth is typically a high temperature process for the metal involved, for example, for Fe above 1000°C and magnesium above 500°C [33].

The rate of oxidation is constant with time

$$\frac{dy}{dt} = c \tag{4.14}$$

while, when integrated, gives

$$y = ct \tag{4.15}$$

with y the oxide thickness, t the time and c a rate constant.

4.4.2 Logarithmic growth

At low temperatures a thin layer of oxide forms that covers the surface. The rate of diffusion through the film is very low and after an initial period of rapid growth, the rate of growth becomes virtually zero.

The rate law can be written as

$$y = c_1 \log\left(c_2 t + c_3\right) \tag{4.16}$$

with y the oxide thickness, t the time and c_1, c_2 and c_3 constants.

Metals which do oxidise in such a manner is magnesium below 200°C and aluminium below 50°C [32].

4.4.3 Parabolic growth

When the oxide film remains intact on the metal surface and forms a uniform barrier the rate of growth of the oxide layer depends on the diffusion of cations and anions through the oxide layer.

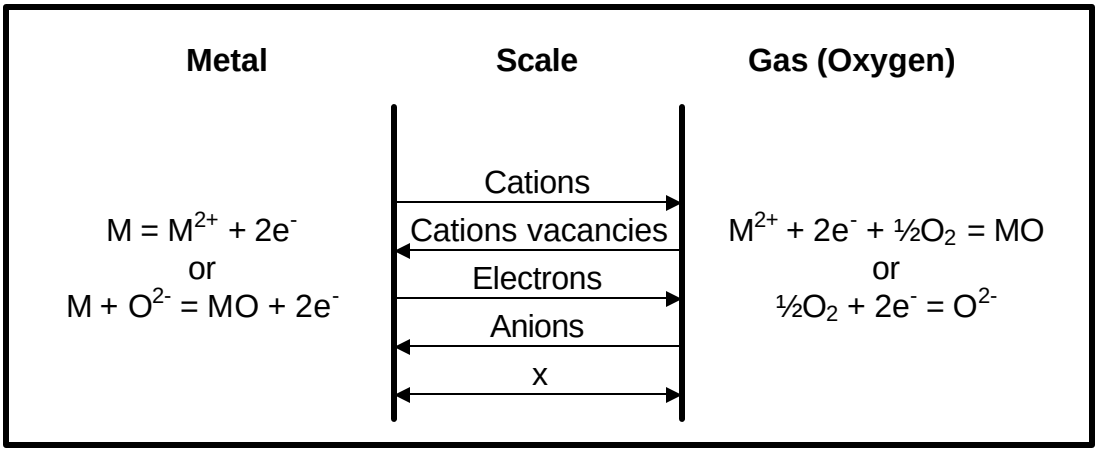

Figure 4.9: Simplified model of diffusion controlled oxidation. [33]

The outward cation flux ($j_{M^{2+}}$) is equal and opposite to the inward flux of cation vacancies. This is shown in figure 4.9. Thus

$$j_{M^{2+}} = -j_{V_M} = D_{V_M} \frac{C_{V_M}^{''} - C_{V_M}^{'}}{x} \qquad (4.17)$$

Where x is the oxide thickness, D_{V_M} is the diffusion coefficient for the cations vacancies and $C_{V_M}^{''}$ and $C_{V_M}^{'}$ are the vacancy concentrations at the scale-gas and scale-metal interfaces respectively.

Since there is thermodynamic equilibrium at each interface, the value $\left(C_{V_M}^{''} - C_{V_M}^{'}\right)$ is constant and thus

$$j_{V_M} = constant \frac{dx}{dt} = D_{V_M} \frac{C''_{V_M} - C'_{V_M}}{x} \tag{4.18}$$

$$\frac{dx}{dt} = \frac{k'}{x} \text{ where } k' = D_{V_M} \frac{C''_{V_M} - C'_{V_M}}{constant} \tag{4.19}$$

Integrating and noting that $x = 0$ at $t = 0$

$$x^2 = 2k't \tag{4.20}$$

which is the common parabolic rate law.

Chapter 5

Experimental Setup

5.1 Introduction

In this chapter the experimental techniques and the procedure of the study is discussed. Most of the techniques are known therefore only a quick oversight of the techniques is given.

In this study only one type of steel was used to eliminate unwanted variables. The study was divided up into two parts and each part was done on a different Auger-systems. The settings on the systems were kept constant during the experiment, in order to directly compare the data of the different experiments.

5.2 Sample Preparation

The samples for this study were disks with a diameter of 1 cm, cut from an industrial flat steel sheet. Thus the preparation process was simplified a little, due to the fact that the sample of the steel that was received was already ready for analysis. Figure 5.1 illustrates the process the steel went through, before the steel was cut into samples.

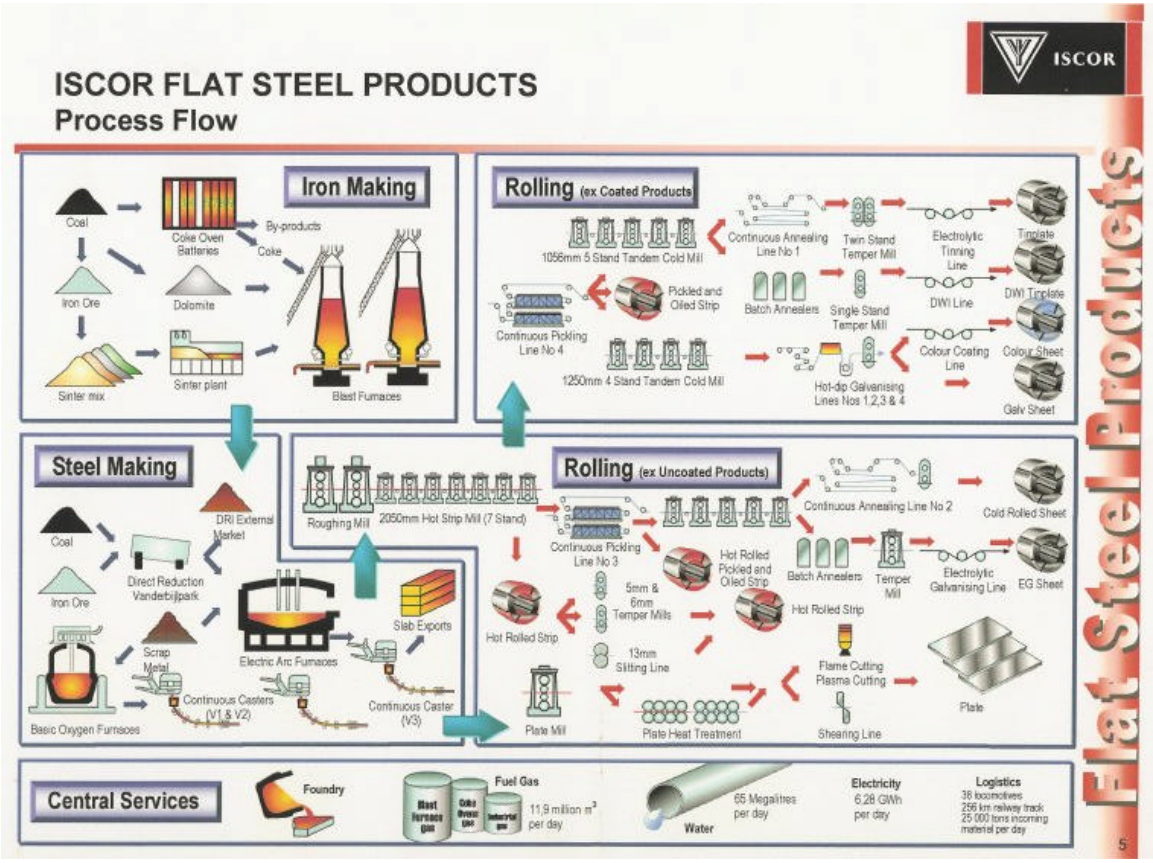

Figure 5.1: Basic steel preparation at ISCOR.

The sample was polished before it was introduced into the AES system. The basic process of sample polishing may be broken up into two parts. First the rough work is done by using a 400 grid sanding paper. This part usually is quick, but also forms more surface defects, usually in the form of “deep” scratches in

the surface. This is followed by the second part, where diamond solutions are used to polish the samples down to a surface roughness of approximately one micron.

5.3 Auger Electron Spectroscopy (AES)

The Auger process is discussed in more detail in the book of Wall [37] and the book of Briggs and Seah [38].

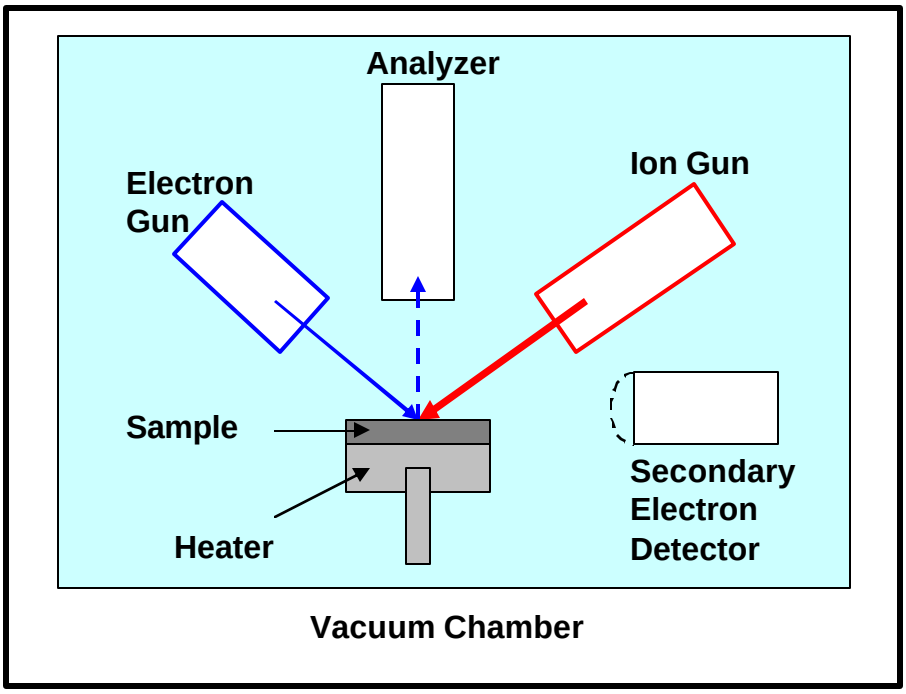

Figure 5.2: Basic components of an AES system [37].

5.3.1 AES 549

In this part only the apparatus and settings that was used during the study is discussed. This apparatus was used for the first part of this study.

Figure 5.3: Photo of the AES 549, which was used during the study.

A photo of the system used during this study is displayed in figure 5.3. The following components of the system were used:

1. Ion Pump: With which the vacuum chamber is pump down to a base pressure of 1 x 10^{-9} Torr.

2. Physical Electronics Electron Gun (PHI Model 11 - 010): The Auger spectra were measured with a primary energy of 3 keV and with the elastic peak at 2 keV. The filament current 3.2 A and the emission current at a constant 5 mA. During the measurement of the Auger spectra the beam current was 20 µA.

3. Double Pass Cylindrical Mirror Analyzer (CMA): The apertures were set to small, due to the high flux of electrons emitted during the Auger process.

4. Physical Electronics Auger System Control (PHI Model 11 - 055): This unit controls the voltages on the cylinders of the CMA, so that only electrons with a certain amount of energy can pass through the CMA. The unit is controlled by a computer, which means that the Auger data is recorded in digital format.

   The energy ranges that were scanned were the following:

   - P (100 eV – 140 eV)
   - S (140 eV – 165 eV)
   - C (245 eV – 285 eV)
   - Ti (345 eV – 435 eV)
   - O (480 eV – 540 eV)
   - Fe (685 eV – 725 eV)

5. Physical Electronics Electron Multiplier Supply (PHI Model 20 - 075): The high voltage supply was set to 1900 V for measuring the Auger data and 1400 V for the elastic peak.

6. Physical Electronics Lock-in Amplifier (PHI Model 32 - 010): During the study a sensitivity of 0.2 mV, a modulation amplitude of 2 eV and a time constant of 0.1 seconds were used and kept constant through out the experiments.

7. Perkin Elmer Ion Gun (11 - 065): The ion gun's emission current was set to 25 mA, a raster area of 4 mm^2 and a voltage of 2 keV.

5.3.2 SAM 590

In the second part of the study the samples were moved to the SAM 590.

Figure 5.4: Photo of the SAM 590, which was used during the study.

In figure 5.4 a photo is displayed of the system that was used for this study. The following components of the system were used:

1. Ion pump: With which the vacuum chamber is pump down to a base pressure of 1 x 10^{-9} Torr.

2. Physical Electronics Electron Gun (PHI Model 18 - 085): The Auger spectra were measured with a primary energy of 3 keV and with the elastic peak at

2 keV. The filament current 1.8 A and the emission current at a constant 20 mA. During the measurement of the Auger spectra the beam current was 5 μA.

4. Single Pass CMA: The apertures were set to medium to let the highest flux of electrons reach the electron multiplier.

5. Physical Electronics Auger System Control (PHI Model 11 - 055): This unit controls the voltages on the cylinders of the CMA, so that only electrons with a certain amount of energy can pass through. The unit is controlled by a computer, which means that the Auger data is recorded in digital format.

   The energy ranges that were scanned were the following:

   - P (100 eV – 140 eV)
   - S (140 eV – 165 eV)
   - C (245 eV – 285 eV)
   - Ti (345 eV – 435 eV)
   - O (480 eV – 540 eV)
   - Fe (685 eV – 725 eV)

6. Physical Electronics Electron Multiplier Supply (PHI Model 20 - 075): The high voltage supply was set to 1700 V for measuring the Auger data and 1200 V for the elastic peak.

7. Physical Electronics Lock-in Amplifier (PHI Model 32 - 010): During the study a sensitivity of 0.4 mV, a modulation amplitude of 2 eV and a time constant of 0.1 seconds were used and kept constant through out the experiments.

8. Perkin Elmer Ion Gun (11 - 065): The ion gun's emission current was set to 25 mA, a raster area of 2.25 mm^2 and a voltage of 2 keV.

5.3.3 Quantitative analysis

It is of vital importance to relate the observed APPH to actual composition of the specimen. The observed signal from an element is not just the average concentration, because it is dependent on the distribution of the element in the first few atomic layers of the surface. Some of the mechanisms responsible of how the crystalline nature of the specimen can influence the intensity of Auger peaks are [37]:

- The composition and density differences of atomic planes parallel to the surface.
- Through anisotropy in the emission process itself or by diffraction of the emitted Auger electrons.
- Channelling effects caused by the diffraction of the exciting electron beam.
- Backscattering of primary electrons.

A good approximation of fractional atomic concentration X_A for element A in a sample is given by [37,38]

$$X_A = \frac{I_A / I_A^{\infty}}{\sum_n I_n / I_n^{\infty}} \qquad (5.1)$$

where I_n is the measured peak height for element n and I_n^{∞} is the measured peak height of the pure standard, recorded under identical conditions. Eq. (5.1) can be rewritten as

$$X_A = \frac{I_A / s_A}{\sum_n I_n / s_n} \qquad (5.2)$$

where I_n is the measured peak height for element n and s_n is the relative atomic sensitivity for the associated peak.

5.4 Heating System

5.4.1 Sample heater

In segregation measurements, the temperature plays a critical role. A method was needed in which the temperature of the sample is kept constant. During this study more than one sample was used, so repeatability between the samples was needed. Due to all these requirements a sample heater was developed. The sample heater is shown in figure 5.5.

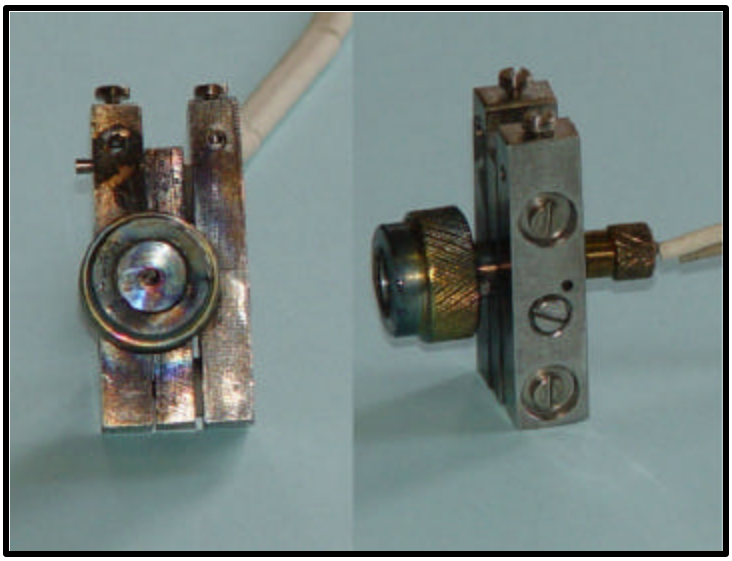

Figure 5.5: Photos of the sample heater used during this study.

The sample heater has the following properties:

- A thermocouple pressing against the back of the sample.

- The thermocouple need not to be changed, even if the sample is changed, thus the results are comparable.
- The samples are easily changeable.
- The filament of the heater stays in tack during the sample change.

5.4.2 Temperature control

This heater was used to heat the sample while AES was used to analyse the sample. In this study the heater control consists of two parts. Firstly a control unit that gives the heater the voltage to heat the sample and then a reference temperature block that gives a more accurate measurement with the thermocouple.

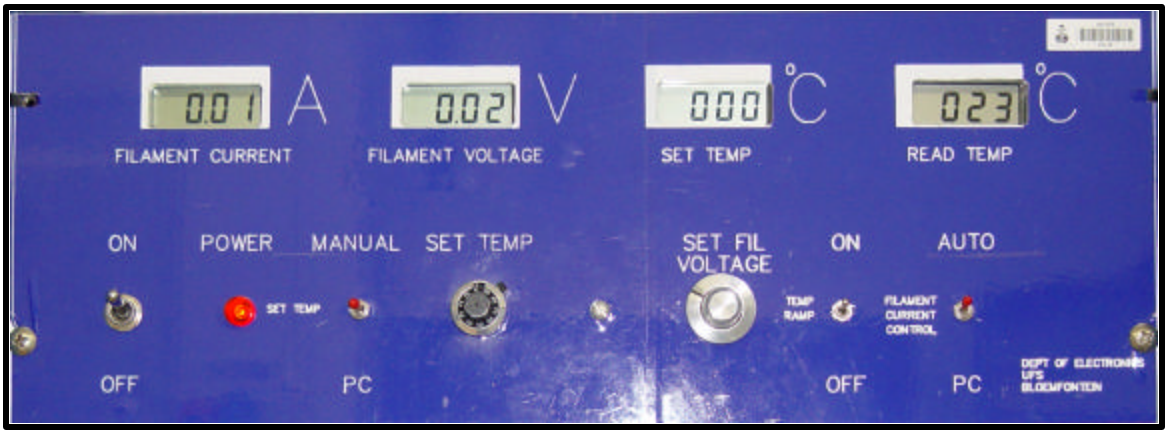

Figure 5.6: Photo of heating control unit.

The heating control unit, shown in figure 5.6, can be controlled manually or with a computer. The unit can either be used for constant temperature or linear heating measurements. Only constant temperature heating was used for this study.

For a more accurate temperature measurement the thermocouple runs through a reference temperature block (see figure 5.7), which is kept constant at a temperature of 35 °C.

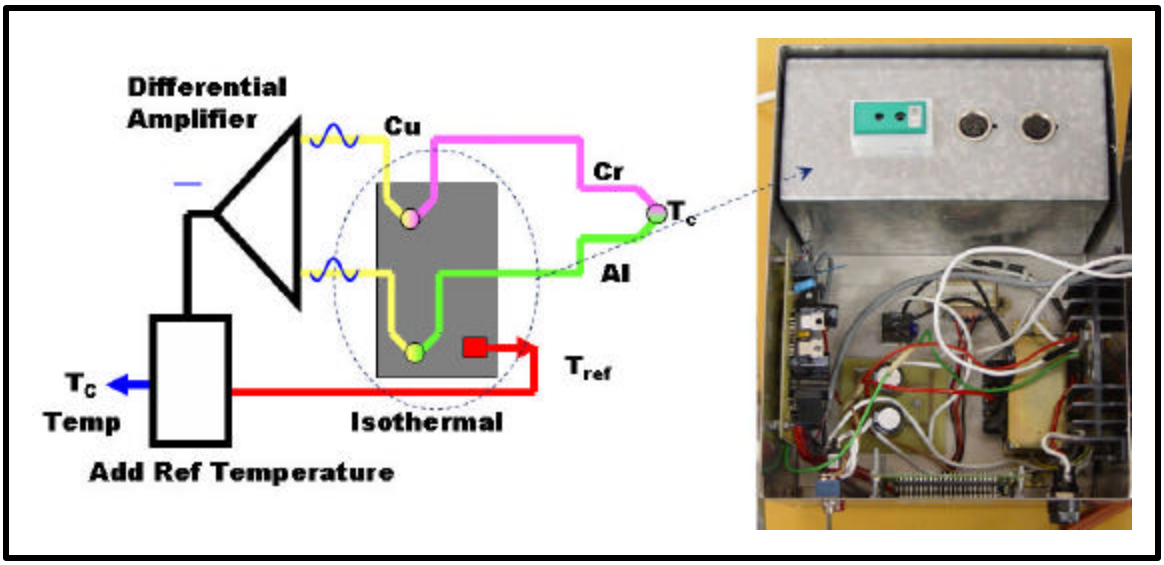

Figure 5.7: Photo of the inside of the reference temperature block.

5.5 Procedure

To keep the segregation data comparable the procedure was kept the same for each experiment.

The following steps were taken during the acquiring of the data:

1. The steel sample was introduced into the vacuum chamber and pumped down to a base pressure of 1 x 10^{-9} Torr.

2. The sample was heated to the required temperature and kept at the constant temperature.

3. After the temperature stabilized the surface was sputtered clean with 2 keV Ar^+ ions.

4. Directly after sputtering the segregation profile was measured, while the Ar^+ was pumped out of the system.

5. Oxygen was introduced after segregation was allowed for some time. Different pressures were used; this pressure (total pressure) was kept constant till equilibrium was reached. (This step is only applicable to the oxidation segregation runs.)

6. The oxygen was pumped out of the system and then the next segregation run was acquired by starting at step 2 in the procedure.

5.6 Linear Least Squares (LLS) Method

The LLS method was used to determine the fractions of the contribution of each element to each point in the depth profile. This method makes use of standards of all the pure elements to determine the contribution of each to a measured Auger spectrum from the sample containing all the standards.

Let $\boldsymbol{a_i}$ be an *1xN* vector containing the spectra of the measured standards. The *ixN* matrix, $\mathbf{A} = [\mathbf{a_1}, \mathbf{a_2}, \ldots, \mathbf{a_i}]$ is constructed. Let each measured spectrum **B**, be an *Nx1* vector containing the Auger spectrum of the combination of the standards.

The 1xi vector $\mathbf{X} = [\mathbf{x}_1, \mathbf{x}_2, \ldots, \mathbf{x}_i]$, with $\mathbf{x}_i$ being the fractions of $\mathbf{a}_i$ in **B**, is the least squares solution to the over-determined system

$$\mathbf{AX} = \mathbf{B} \qquad (5.3)$$

given by [39]

$$\mathbf{X} = (\mathbf{A}^T\mathbf{A})^{-1}\mathbf{A}^T\mathbf{B} \qquad (5.4)$$

The reconstructed **B** matrix is given by

$$\mathbf{B} = \mathbf{x}_1\mathbf{A} + \mathbf{x}_2\mathbf{A} + \ldots + \mathbf{x}_i\mathbf{A}$$

In the next chapter the experimental data is discussed.

Chapter 6

Results and Discussion

6.1 Introduction

In this chapter the results of the segregation of alloying elements in an ULC industrial steel are discussed. In chapter 4 the influence of oxygen on segregation is discussed. The aim of the experimental results is to determine the influence of oxygen on the segregation process.

The following experiments were done:

1. Firstly the segregating species were identified.

2. Then AES data was measured to determine the temperature dependence of the oxygen-induced segregation.

3. The AES data was measured to get the influence of the oxygen pressure on segregation kinetics.

4. Finally a simulation was done to show that a correlation between the oxygen-induced segregation theory and the experimental results exists.

6.2 Identification of Segregated Elements

During the production of sheet steel several elements are trapped in the bulk material, for specific metallurgical reason. The elements trapped in the steel used for this study are shown in table 6.1.

Element	Element wt%
Al	0.03100
B	0.00040
C	0.00220
Cr	0.03000
Cu	0.01000
Mn	0.12900
Mo	0.00900
N	0.00280
Ni	0.02000
P	0.01600
S	0.00700
Si	0.00700
Sn	0.00100
Ti	0.07800
V	0.00500

Table 6.1: Specific wt% concentration values of the trapped elements in flat steel, obtained with inductively coupled plasma (ICP).

The segregation elements were determined from the Auger spectrum after the steel sample was heated at a constant temperature of 700 °C for 24 hours. The spectrum is shown in figure 6.1.

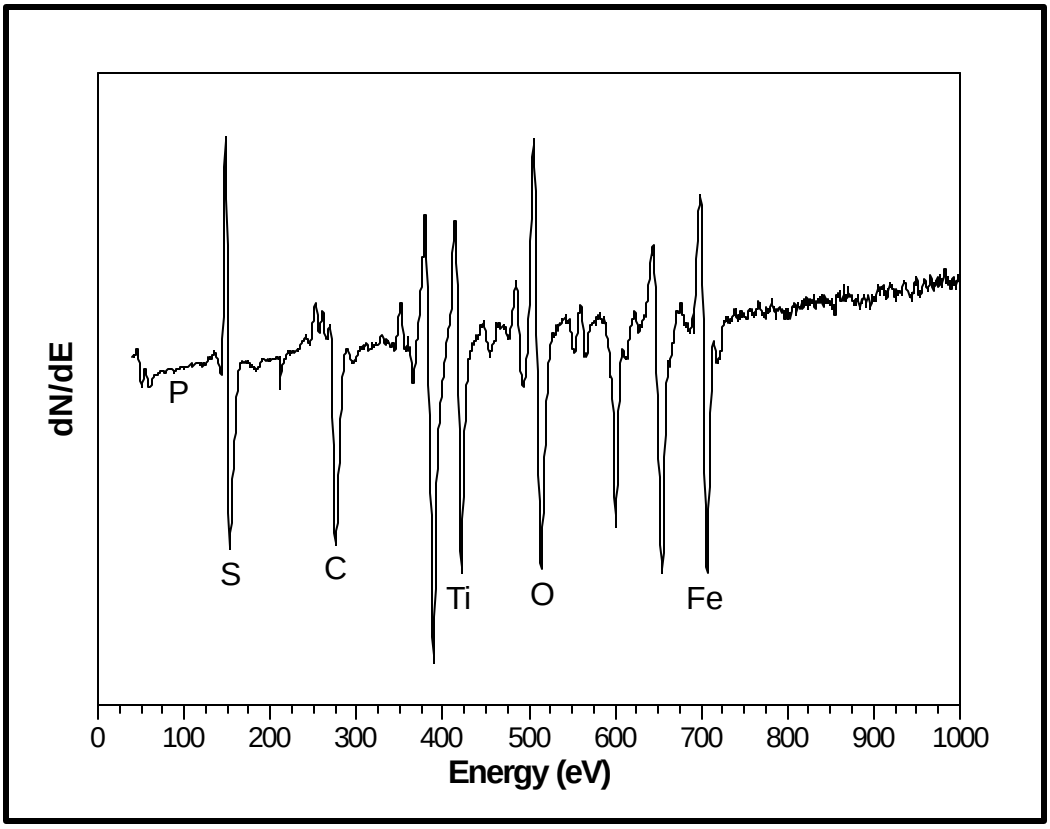

Figure 6.1: Auger spectrum of steel sample, after 24 hours annealing at 700 °C.

The segregation elements were P, S, C and Ti with all the Auger energies shown in table 6.2. Although no P was observed after 2 hours, the P initially segregated to the surface.

Element	Energy (eV)	Element	Energy (eV)
P	123	Ti	421
S	153	O	510
C	275	Fe	705

Table 6.2: Obtained Auger energies for the segregated species and bulk elements.

6.3 Quantifying the Auger data

In chapter 5 two equations were given for quantification. The first is dependent on the peak height of pure standards of all elements measured under the exact conditions as the experiments were done. In the industrial sample there are many different elements, with many of which the pure standards was unavailable. Thus the second equation was used for all of the analysis, with the relative atomic sensitivity factors were taken from the Handbook of Auger Electron Spectroscopy [40]. The sensitivity factors that were obtained are tabulated in table 6.2.

Element	Sensitivity Factor
P	0.83
S	1.35
C	0.17
Ti	0.52
O	0.34
Fe	0.26

Table 6.2: Relative atomic sensitivity factors for all elements used to quantify the Auger data.

6.4 Temperature Dependence of Oxygen-Induced Segregation

The different impurity elements were monitored with the help of a multiplexer program during the acquirement of the segregation profile. The low energy electron peak of Fe was monitored before and after each segregation profile. The oxidation state of the Fe was determined with the help of this peak. The Auger Peak - to - Peak Heights (APPH's) as a function of annealing time were monitored.

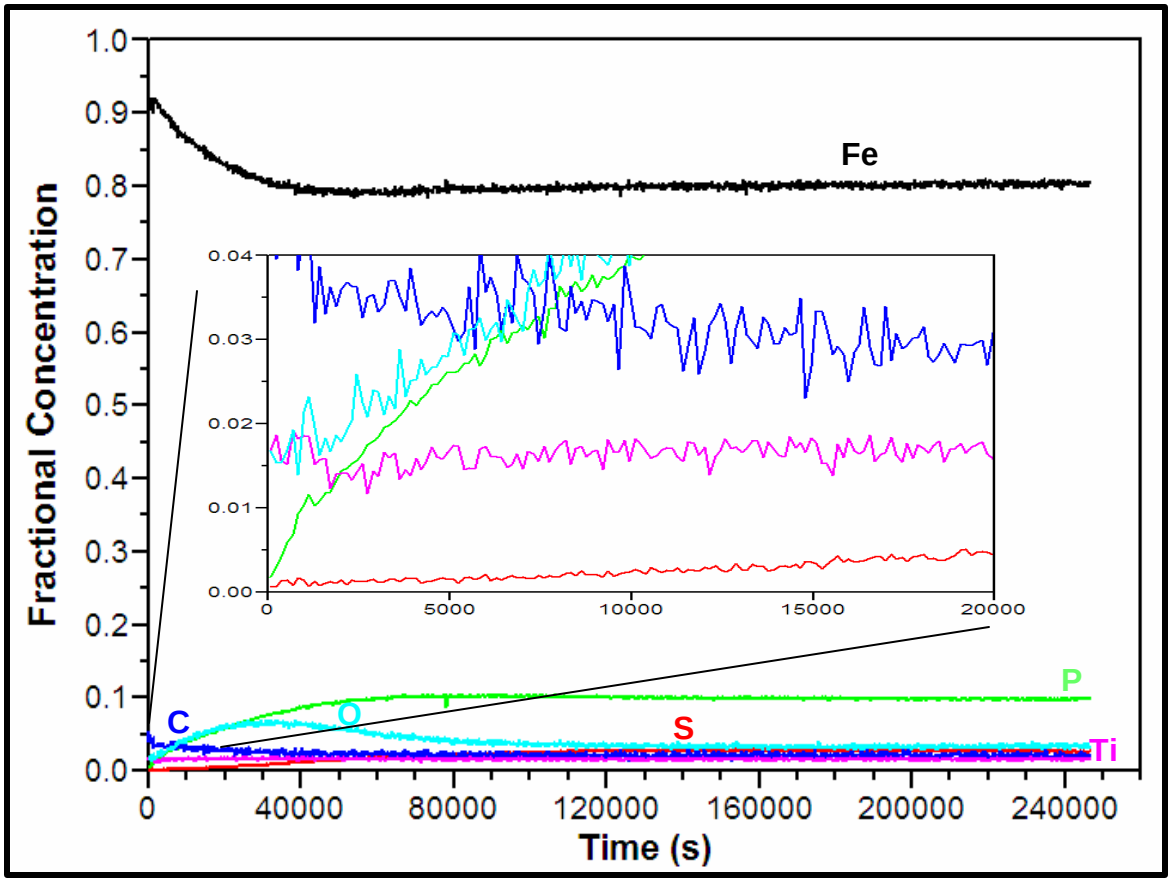

Figure 6.2: APPH's versus time at a temperature of 550 °C.

In figure 6.2 the changes in APPH's that were obtained during the annealing of the sample at a constant temperature of 550 °C, at UHV (< 2 x 10^{-9} Torr) as control sample for the oxygen-induced segregation profiles are shown. The amount of Fe on the surface decrease rapidly as the impurity elements P and Ti segregates to the surface. At the beginning of the profile Ti increase at the surface, and then decreased steadily with time. The S concentration on the surface also starts to increase. The amount of P decreased with the increase of the S concentration. An increase of O was also measured in the beginning.

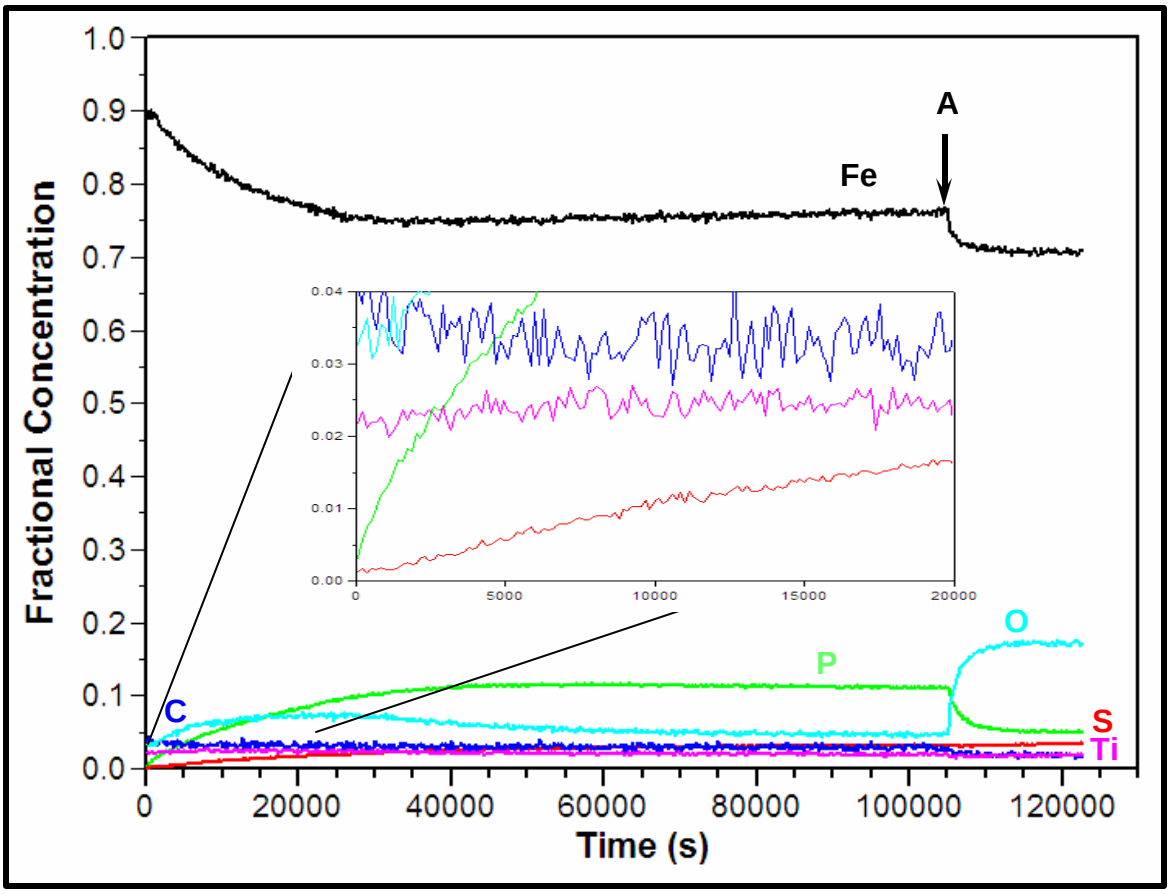

Figure 6.3: APPH's versus time at a temperature of 550 °C. Oxygen was introduced at position A to a pressure of 5 x 10^{-8} Torr.

In figure 6.3 the APPH's are displayed that were obtained during the annealing of the sample at a constant temperature of 550 °C. The first part of the curve

follows the same profile than in figure 6.2 as expected. The systems total pressure was adjusted to 5 x 10^{-8} Torr by leaking O_2 into the system at position A. There was an immediate change in the APPH's with the introduction of oxygen. At this point the amount of O on the surface started to increase rapidly, while Fe, P, Ti and C started to decrease. There was no immediate change in S surface concentration. The low energy spectrum of Fe that was taken directly after the APPH profile is shown in figure 6.4.

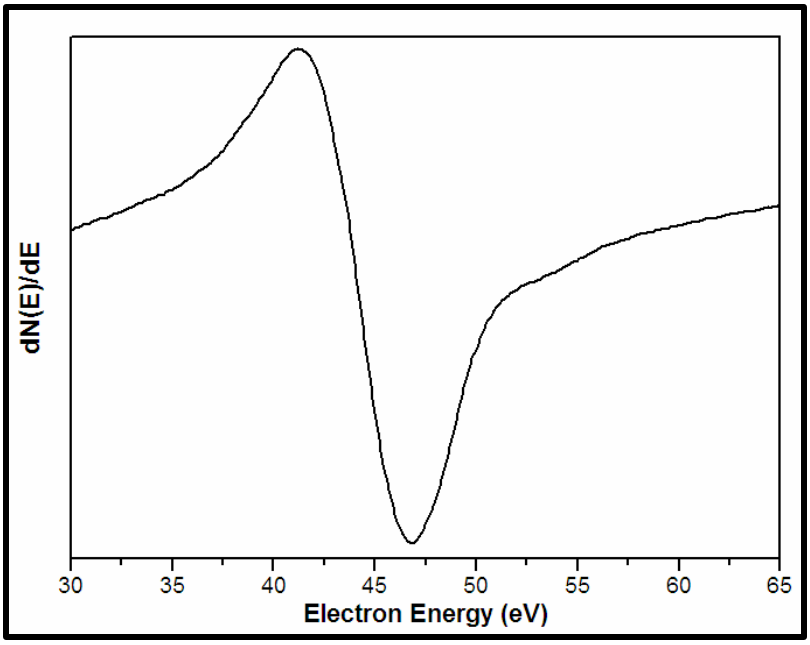

Figure 6.4: Low energy peak of Fe measured after the APPH profile in figure 6.3.

This Fe – peak shows a single peak at electron energy value in the region of 47 eV, which shows that no oxide was formed during the annealing process, as predicted by the phase diagram in chapter 4. This experiment was repeated at 700 °C.

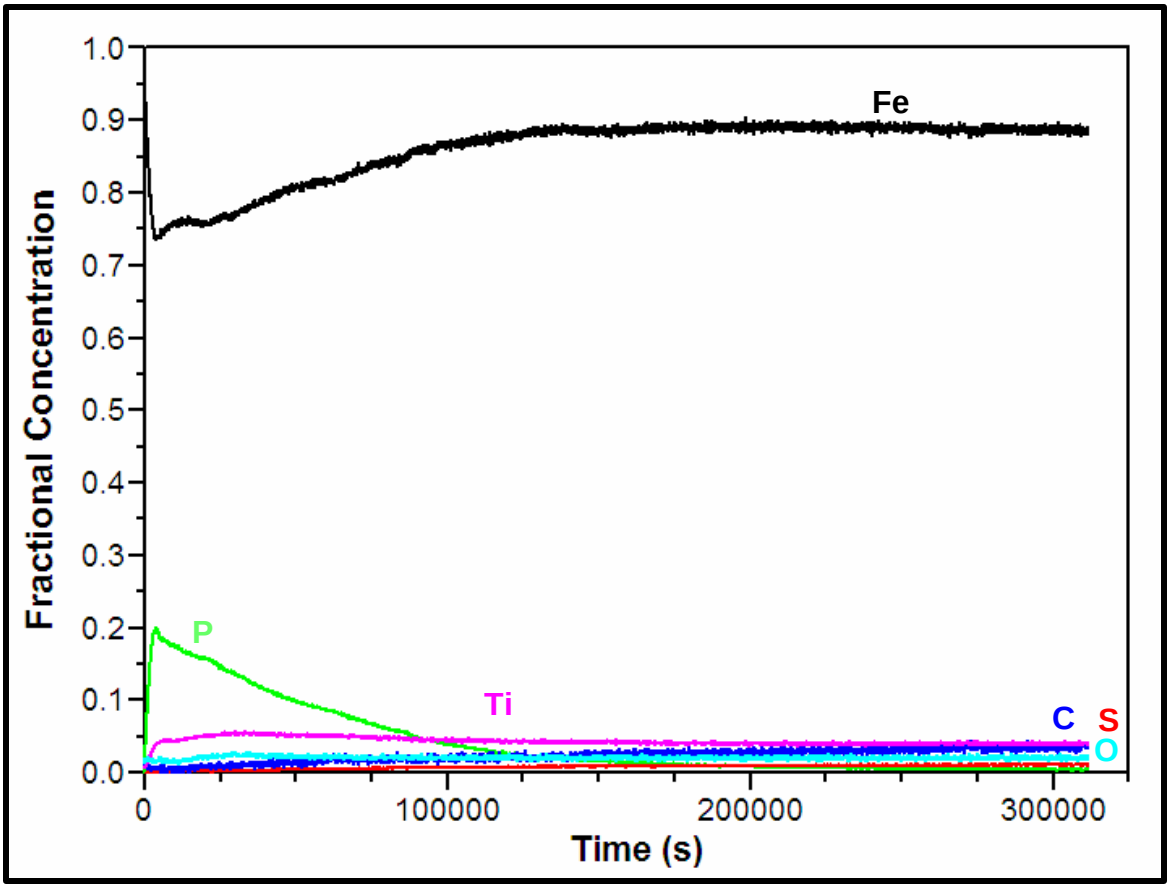

Figure 6.5: APPH's versus time at a temperature of 700 °C.

In figure 6.5 the APPH's that were obtained during the annealing of the sample at a constant temperature of 700 °C are displayed. The amount of P and Ti on the surface increased rapidly, while the amount of Fe decreased. After the initial increase of Ti on the surface the surface concentration decreased steadily. With time the S concentration slowly started to increase and it cause the P surface concentration to decrease. There is no change in the amount of C and O on the surface.

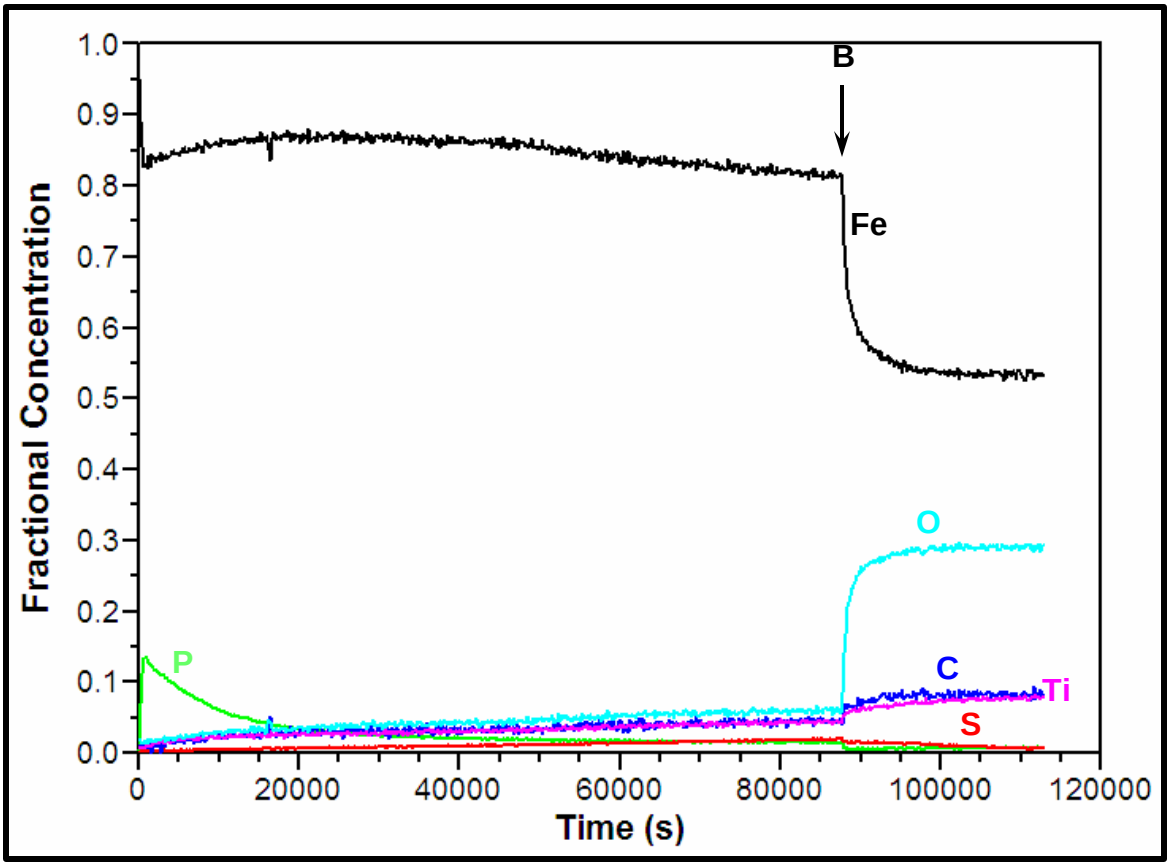

Figure 6.6: APPH's versus time at a temperature of 700 °C. Oxygen was introduced at position B to a pressure of 5 x 10^{-8} Torr.

In figure 6.6 the obtained APPH's are displayed. The same procedure was followed as previously, except that the temperature was increased to a constant temperature of 700 °C. The APPH profile of figure 6.6 follows the same trend than that of figure 6.5. The total pressure of the system was increased to a pressure of 5 x 10^{-8} Torr at point B, by leaking O_2 into the system.

At the point where the O_2 is leaked into the system the surface concentration of O increases rapidly. With the O increase the amount of S, P and Fe decrease on the surface and the Ti started to segregate to the surface, with the increase of the Ti concentration on the surface the C also started to segregate at a low rate and the Fe and S still decreased. The Auger peak of C that segregated during

the oxidation process is illustrated in figure 6.7. The triple peak proves that the C that segregated is a carbide and not pure carbon.

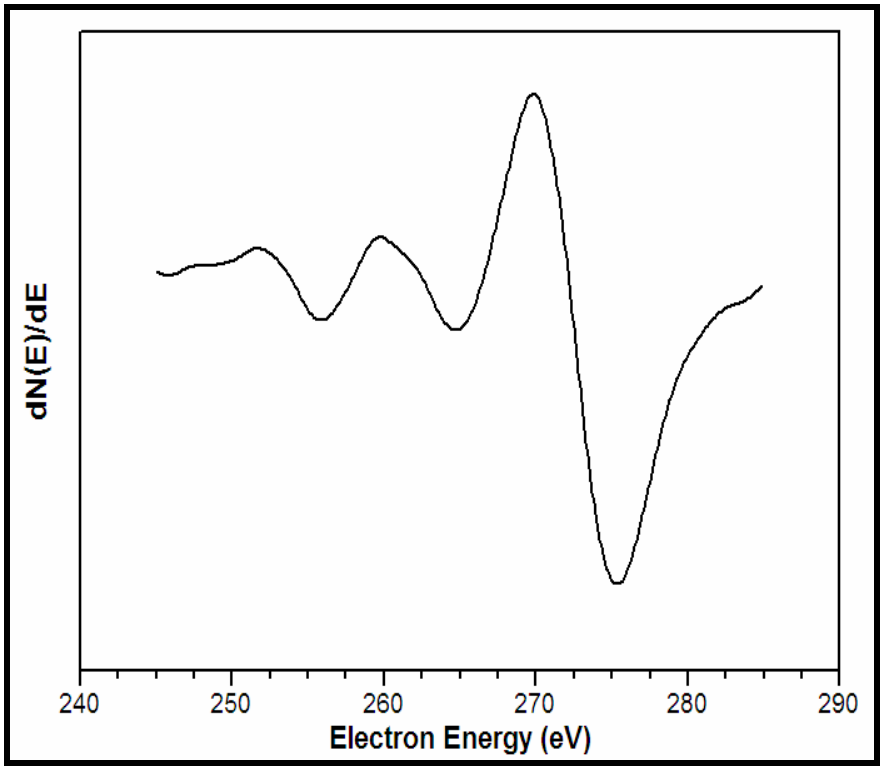

Figure 6.7: Profile of carbon after APPH profile in figure 6.6.

After the APPH profile the low energy peak of Fe was again monitored and is shown in figure 6.8.

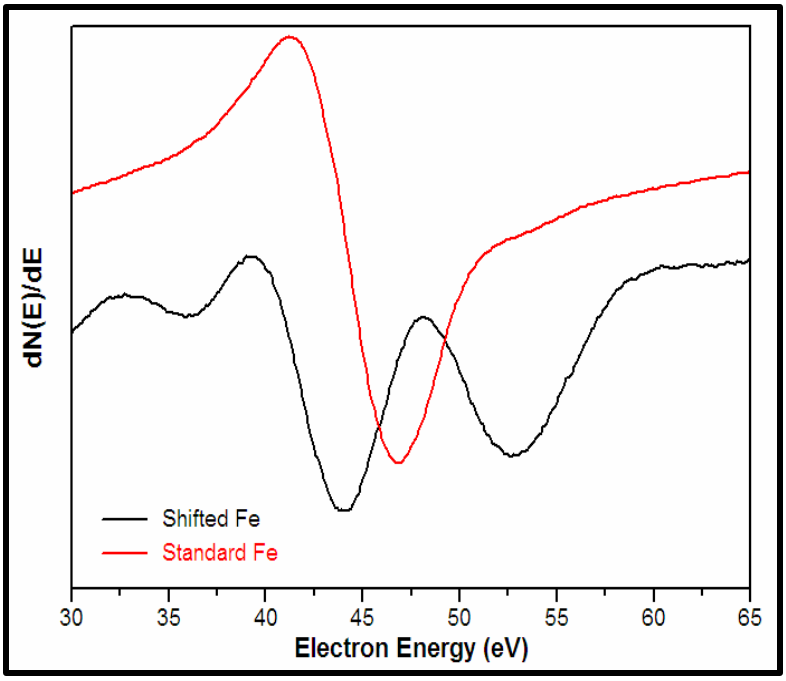

Figure 6.8: Low energy Auger peak of Fe measured at the end of the profile in figure 6.6.

This low energy Fe – peak shows a double peak at the electron energy value of 44 and 53 eV, which shows that iron oxide have formed during this experiment.

6.5 Oxygen Pressure Dependence of Oxygen-Induced Segregation

In this part of the study the same impurity elements, which were monitored in section 6.2, were monitored again.

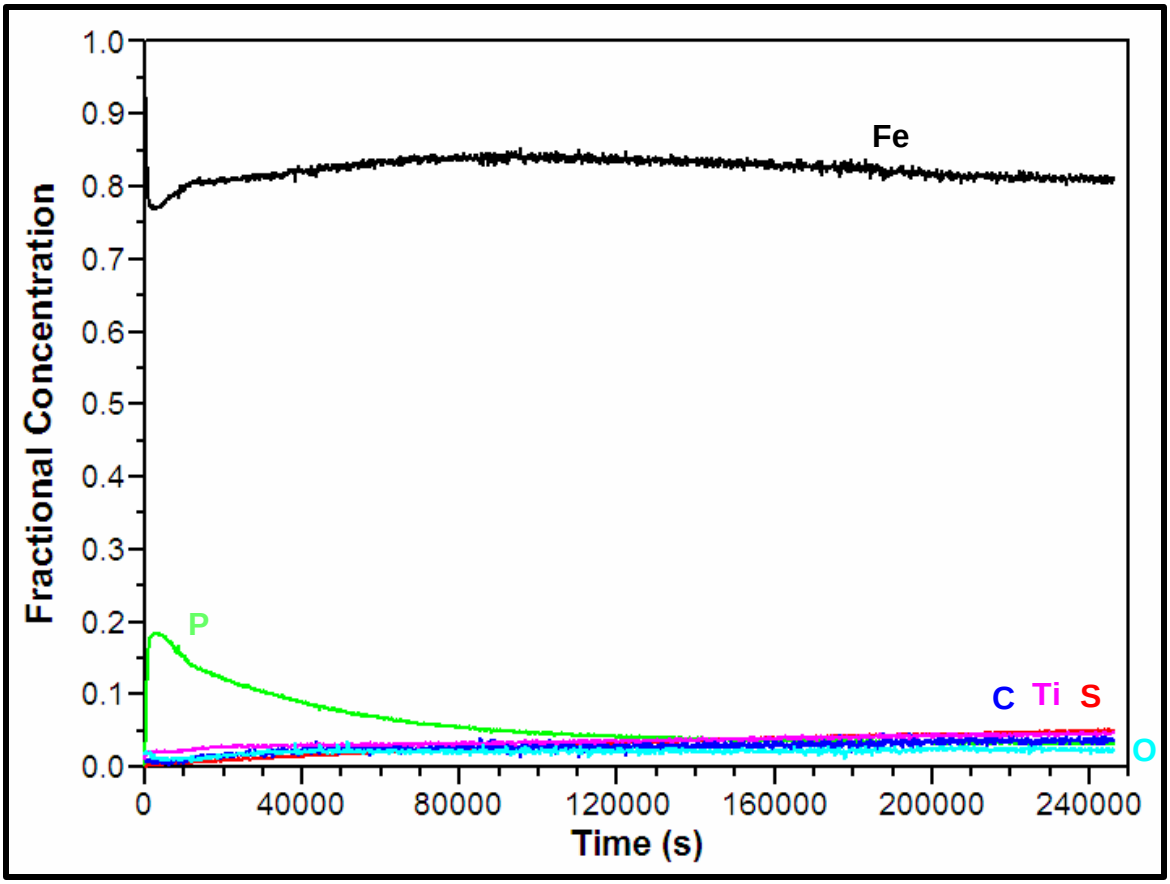

Figure 6.9: APPH's versus annealing time at a temperature of 800 °C.

In figure 6.9 the segregation profile is displayed that was obtained during the annealing of the sample at 800 °C. With the initial segregation of P and Ti the concentration of Fe on the surface slowly decreases. Due to the low segregation rate of S the amount of P on the surface slowly decrease as the S concentration increase. The concentration of C and O on the surface is unchanged during the whole segregation profile.

In figure 6.9 no O_2 was introduced into the system, so the presence of O on the surface is due to the background gases. The experiment was repeated at 800 °C, with different oxygen pressures to determine the dependence on oxygen pressure. The pressures that were used were 5 x 10^{-9} Torr, 1 x 10^{-8} Torr, 5 x 10^{-8} Torr and 1 x 10^{-7} Torr.

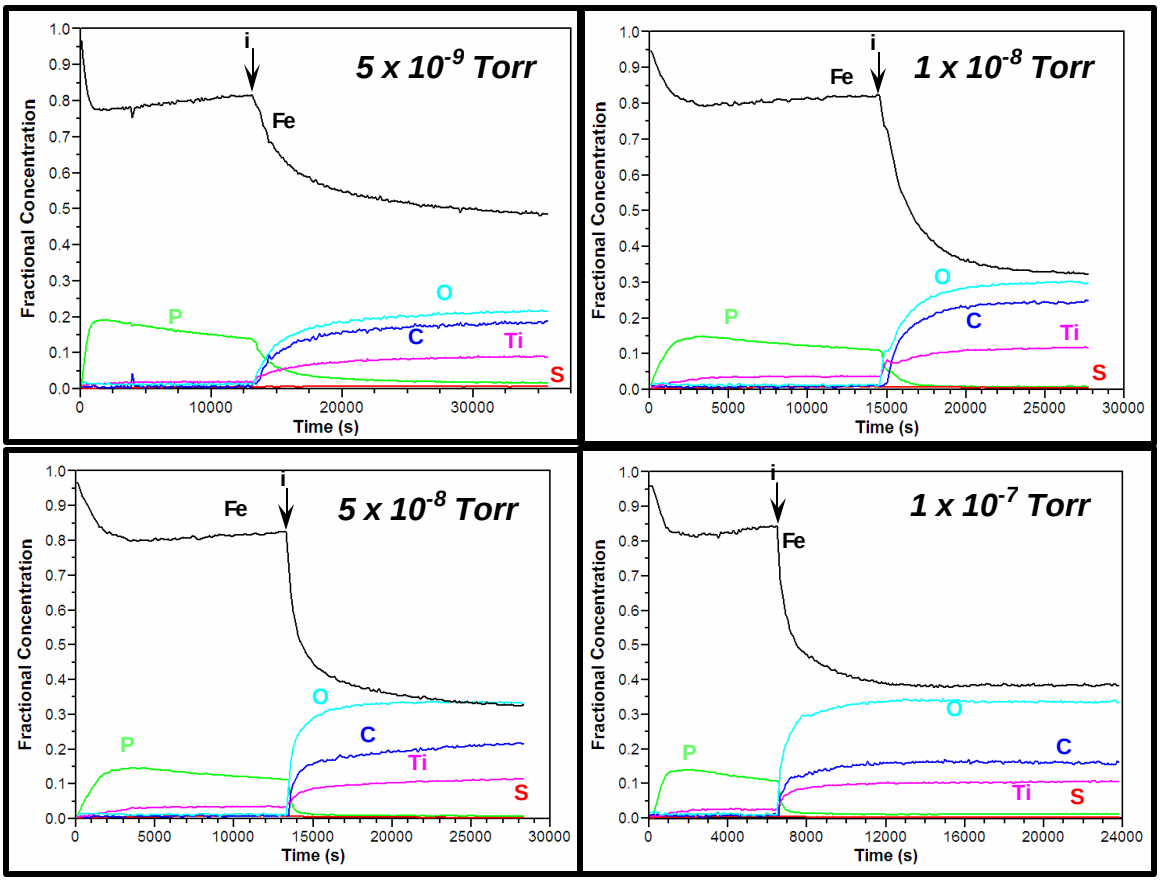

Figure 6.10: Fractional surface concentration versus annealing time at temperature of 800 °C for different pressures of oxygen.

In figures 6.10 the basic profile stayed the same initially without oxygen present in the system, except for the small change in the P concentration. This can be due to grain growth of materials at high temperatures and the fact that it is an industrial sample and not a single crystal. P segregated rapidly to the surface. After the initial segregation of Ti, the surface concentration of Ti remained relatively constant, while the concentration of P decreased as S slowly segregated to the surface. As soon as oxygen is introduced into the system, at position *i*, the concentration of O on the surface increase as the concentration of Fe and P decrease. As soon as O was introduced the Ti and C started to segregate.

The measured Auger spectrum for C at position *i* has a carbide shape shown in figure 6.7 earlier in the chapter. The carbide peak showed that the carbon is apparently never in graphite form, but in a chemical bond. In order to determine the influence of oxygen on the system the Ti peak was not treated as coming from the pure Ti element but as a combination of peaks (Ti, TiN, TiC, TiO and TiO_2) due to the chemical bonds.

To extract the amount Ti in the chemical bond from the measured data, the LLS method that was discussed in chapter 5 was applied. The LLS method is dependent on spectra from standard samples. The spectra of pure samples of Ti and Ti in different chemical bonds (obtained from Goodfellow England) are shown in figure 6.11. The pure samples measured were Ti, TiC, TiN, TiO and TiO_2.

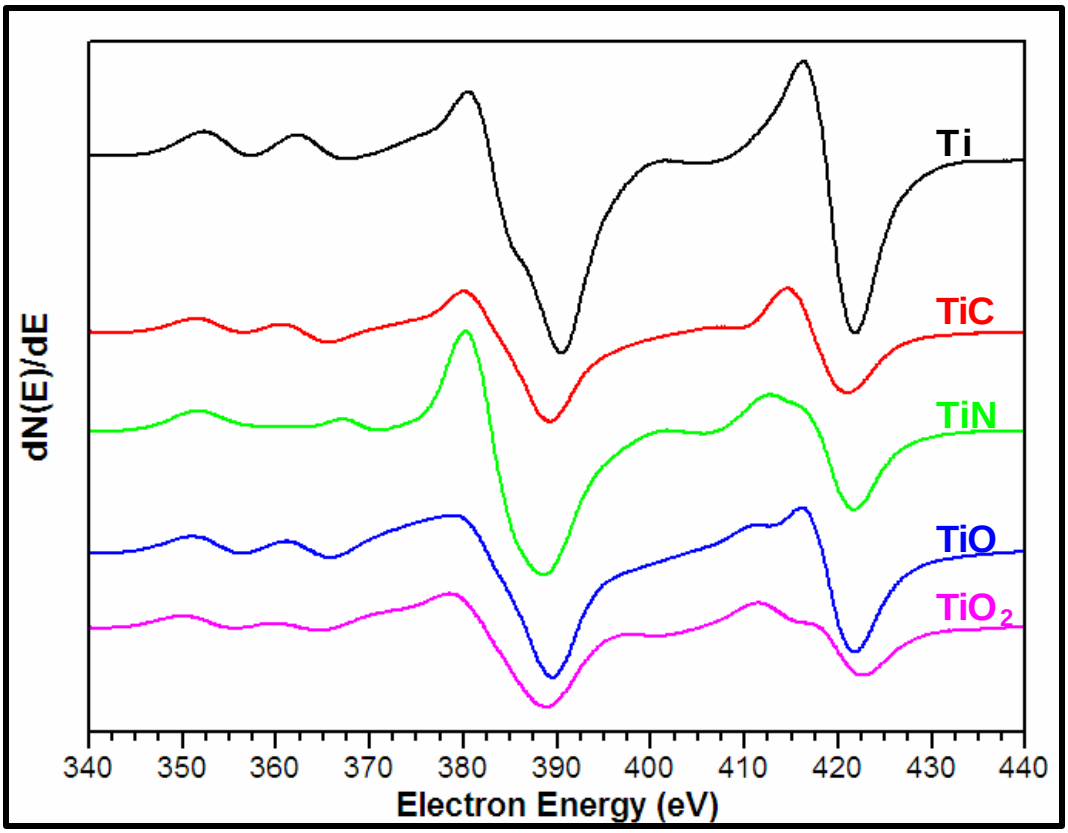

Figure 6.11: Measured Auger spectrum for Ti standards.

The measured Ti Auger spectra were compared to the standards and some of the standards were eliminated, by comparing basic peak shapes. The standards, Ti, TiC, TiN and TiO were used in the LLS equation to extract the contributions of the individual Ti peaks. The LLS equation in chapter 5 can be rewritten as

$$\mathbf{X} = (\mathbf{A}^T\mathbf{A})^{-1}\mathbf{A}^T\mathbf{B} \tag{6.1}$$

where $\mathbf{X} = [\mathbf{x}_{Ti}, \mathbf{x}_{TiC}, \mathbf{x}_{TiO}]$ a 1x3 vector, with $\mathbf{x}_i$ being the fractions of $\mathbf{a}_i$ in **B**, **A** a 3x*N* matrix, consisting of three standards and **B** the measured Ti peak. The contribution of the different Ti is given by

$$\mathbf{AX} = \mathbf{B} \tag{6.2}$$

To reconstruct the measured spectrum, **B** is given by

$$\mathbf{B} = \mathbf{x}_{Ti}\mathbf{A} + \mathbf{x}_{TiC}\mathbf{A} + \mathbf{x}_{TiO}\mathbf{A} \tag{6.3}$$

If any of the fractions is negative that element is ignored and the fractions are recalculated without that elements standard. In figure 6.12 the reconstruction is shown, with the original measured spectrum and the different fractions of the standards that are used to reconstruct the measured spectrum.

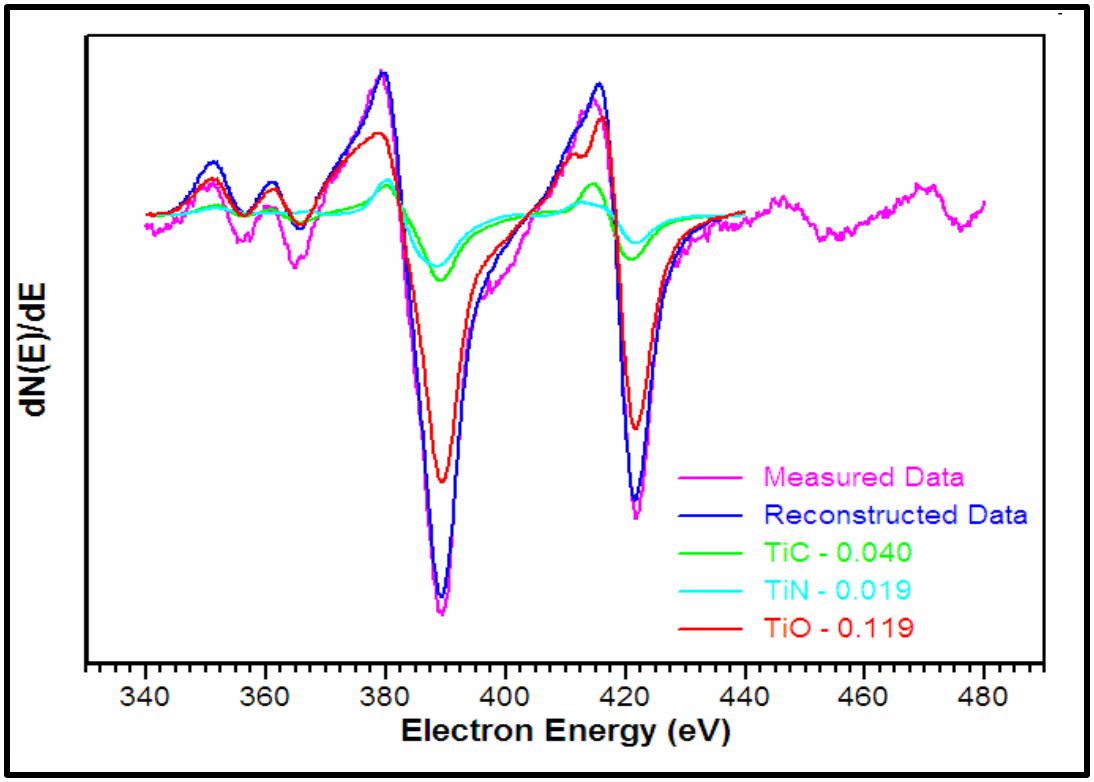

Figure 6.12: Illustration of the applied LLS method.

In figure 6.12 the fractions of individual Ti peaks, the measured and reconstructed Ti peak was compared and the small changes may be due to the fact that no negative fraction $\mathbf{x}_i$ was allowed in the calculations and as soon as $\mathbf{x}_i$ became negative it was forced to zero.

This method was applied to each point of the Auger profile and figure 6.13 was obtained from the data.

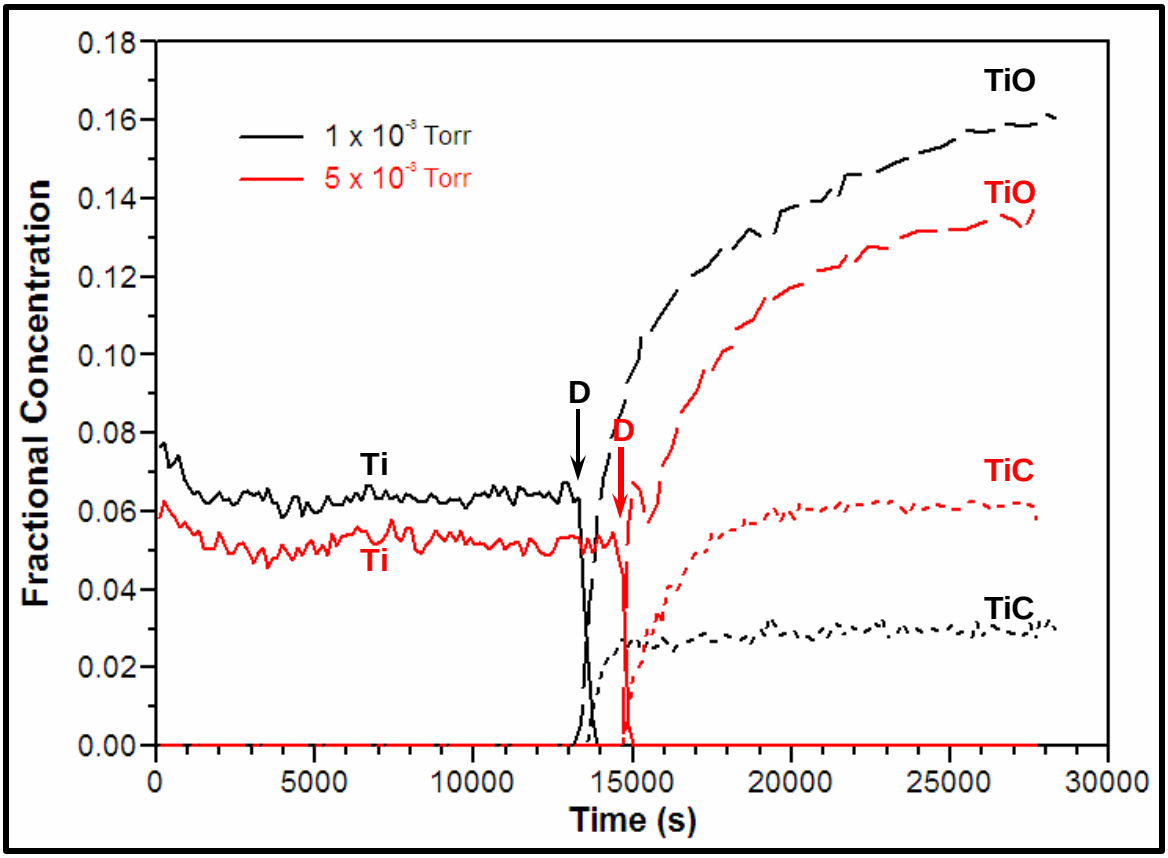

Figure 6.13: Reconstructed Auger profile of Ti for 1 x 10^{-8} Torr and 5 x 10^{-8} Torr.

From figure 6.13 it is clear that initially the Ti is a pure Ti peak. As soon as oxygen is leaked into the system at position D, the pure Ti peak decreased with a subsequent increase in TiO and TiC. There was a small time difference between the increase of the TiO and the increase of the TiC, which indicate that the oxygen caused the Ti to segregate and the Ti caused the C to segregate. The amount of TiC also increased with an increase of oxygen pressure.

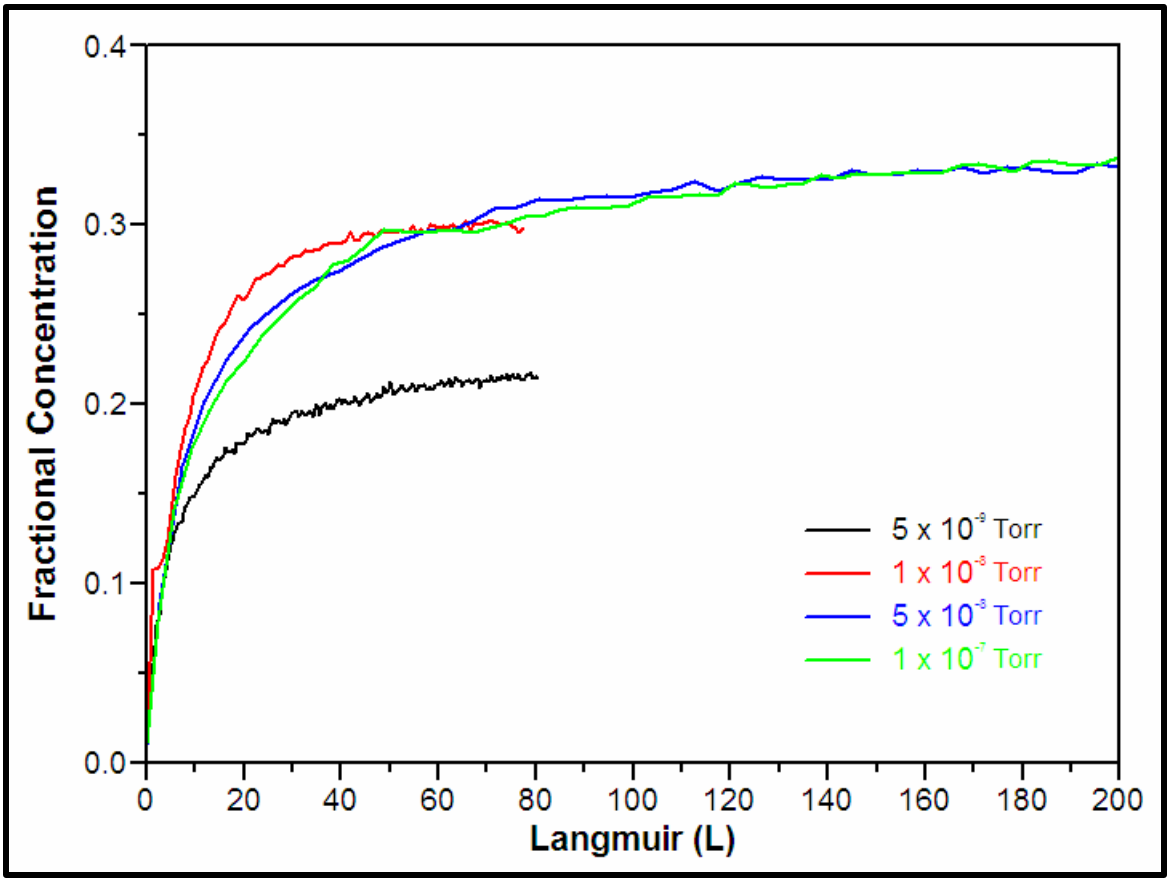

Figure 6.14: Manipulated O data as a function of Langmuir.

In figure 6.14 the fractional concentration as a function of oxygen coverage in Langmuir is displayed, for the oxygen rich part of the study. It shows that the gradient of increase stayed constant for this study. This shows that the oxidation mechanism stayed constant during the study, with the change in oxygen pressure.

6.6 Oxidation and Segregation

In chapter 3 segregation is discussed and in chapter 4 oxidation is discussed, in the following part these two parts will be combined and the effect of oxidation during segregation will be discussed.

Under equilibrium conditions the modified Darken equation can be reduced to the Guttman equations [15,20].

$$X_1^f = \frac{X_1^B \exp(\Delta G_1 / RT)}{1 - X_1^B + X_1^B \exp(\Delta G_1 / RT) - X_2^B + X_2^B \exp(\Delta G_2 / RT)}$$
$$X_2^f = \frac{X_2^B \exp(\Delta G_2 / RT)}{1 - X_1^B + X_1^B \exp(\Delta G_1 / RT) - X_2^B + X_2^B \exp(\Delta G_2 / RT)} \quad (6.3)$$

where

$$\Delta G_1 = \Delta G_1^0 + 2\Omega_{13}(X_1^B - X_1^f) + \Omega'(X_2^f - X_2^B)$$
$$\Delta G_2 = \Delta G_2^0 + 2\Omega_{23}(X_2^B - X_2^f) + \Omega'(X_1^f - X_1^B) \quad (6.4)$$

with X_i^B and X_i^f are the bulk and surface concentrations of species *i*. The interaction parameter between species *i* and the solvent 3 is given by Ω_{i3} and $\Omega' = \Omega_{12} + \Omega_{23} + \Omega_{13}$.

In equation 6.4 the segregation energy equations are stated. Species 1 is taken as oxygen, 2 as any other impurity and 3 the matrix element, Fe. If no oxygen is present in the system the segregation energy of specie 2 is lower as it is with oxygen in the system due to the fact that the concentration $\left(X_2^f\right)$ is zero.

If the concentration of oxygen increases the segregation energy will also increase. If the concentration of oxygen and the other two species stays the same the segregation energy will change. This will determine what element will occupy the surface.

6.7 Simulating Oxygen Induced Segregation

The next step is now to get a correlation between theory and experimental data. From this industrial steel that has a high amount of impurities elements, the simulation can be very difficult, due to the fact that the modified Darken model gets rather complicated. So for this part the system was taken as a ternary system.

The three elements that were considered was Fe, because it is the bulk element, oxygen (to see if the oxygen induced segregation can be simulated) and then the other element can be any impurity element.

The modified Darken model is discussed in chapter three and six and the equations in chapter 6.6 were used in a program written by Terblans (see figure 6.15).

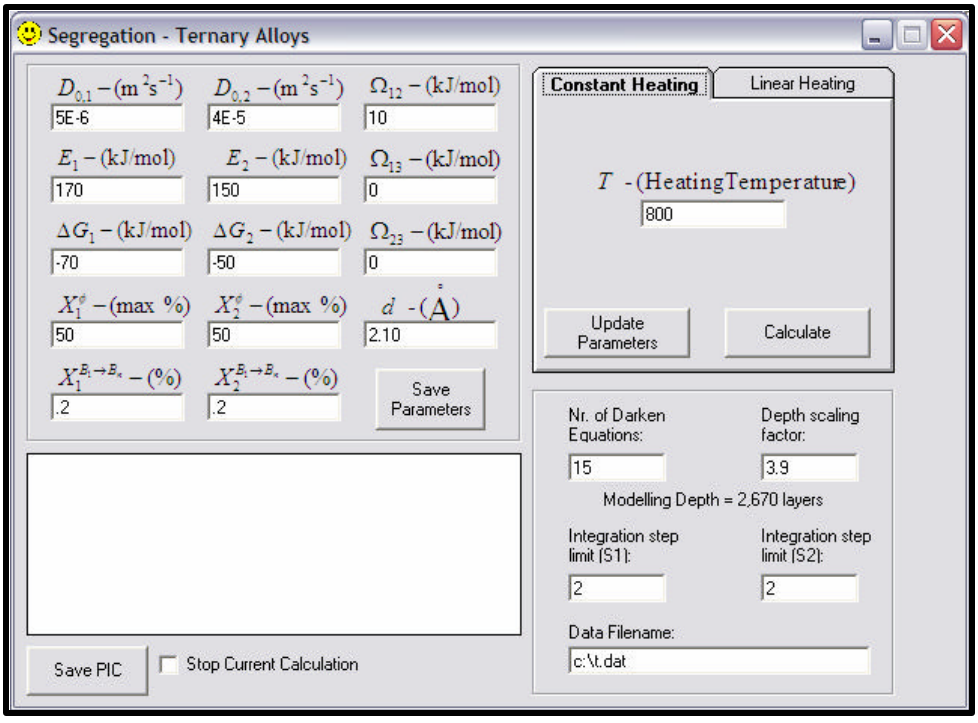

Figure 6.15: Screen capture of program used for the simulations.

In the beginning of a segregation run there is no O_2 in a system which leads to certain DG values, as soon as the O_2 is introduced both species 1 and 2 DG values will change, due to the change in oxygen concentration on the surface. In figure 6.16 the results of one of the simulation are shown.

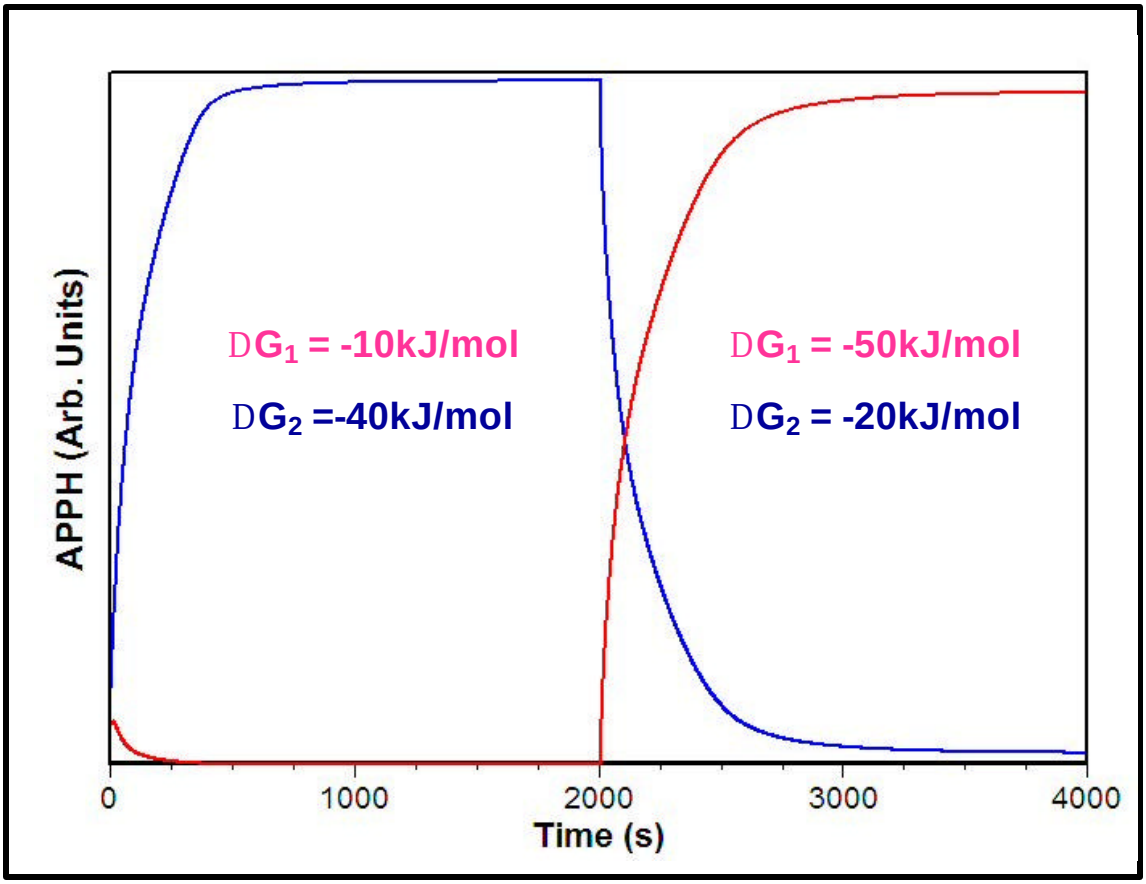

Figure 6.16: Theoretical data from the modified Darken model.

Let the first 2000 seconds in figure 6.16 be without oxygen and the next 2000 seconds (highlighted area) be an oxygen rich system. In the beginning element 1 (red) starts to segregate, but as soon as element 2 (blue) goes to the surface it displace the 1st element on the surface. As soon as the atmosphere is changed element 1 starts to segregate again and displaces the 2nd element on the surface, due to the new segregation values.

The next step is to find the change in segregation energy as a function of oxygen surface coverage.

6.8 Oxidation Kinetics

In chapter 3 the basics of segregation is discussed, in particular the Langmuir-McLean equations in chapter 3.3.1. The segregation equation is for a binary system.

$$\frac{X_1^f}{1-X_1^f} = \frac{X_1^B}{1-X_1^B}\exp\left(\frac{\Delta G}{RT}\right) \tag{6.6}$$

In the case of oxidation the surface coverage must be introduced to indicate the role of oxygen on the segregation energy. In figure 6.17 it is shown that with oxygen in the system, the system becomes a mixture between a binary and a ternary system.

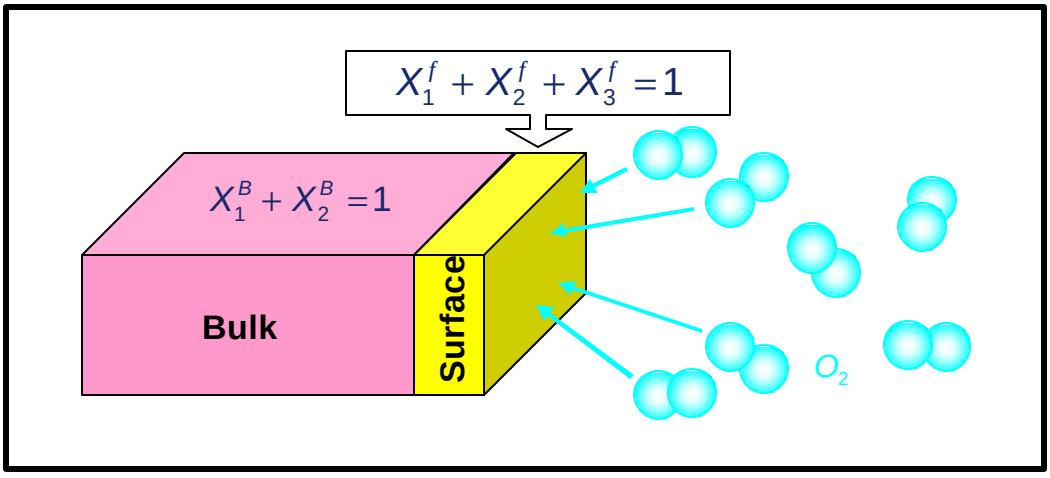

Figure 6.17: Basic illustration of system.

For binary bulk the following assumption is made:

$$X_1^B + X_2^B = 1 \tag{6.7}$$

and for the surface:

$$X_1^f + X_2^f + X_3^f = 1. \tag{6.8}$$

To simplify the mathematics eq. (6.8) has to be satisfied. Even with this statement not completely true in practice, the assumption is still valid.

If we take the equation for a binary system from chapter 3

$$m_1^f - m_1^B - m_2^f + m_2^B = 0 \tag{6.9}$$

with

$$\begin{aligned} m_1^f &= m_1^{0,f} + \Omega_{12}\left(X_2^f\right)^2 + RT\ln\left(X_1^f\right) \\ m_1^B &= m_1^{0,B} + \Omega_{12}\left(X_2^B\right)^2 + RT\ln\left(X_1^B\right) \\ m_2^f &= m_2^{0,f} + \Omega_{12}\left(X_1^f\right)^2 + RT\ln\left(X_2^f\right) \\ m_2^B &= m_2^{0,B} + \Omega_{12}\left(X_1^B\right)^2 + RT\ln\left(X_2^B\right) \end{aligned}. \tag{6.10}$$

Substituting eq. (6.10) into eq. (6.9), it follows that

$$\begin{pmatrix} m_1^{0,f} + \Omega_{12}\left(X_2^f\right)^2 + RT\ln\left(X_1^f\right) - m_1^{0,B} - \Omega_{12}\left(X_2^B\right)^2 - RT\ln\left(X_1^B\right) \\ -m_2^{0,f} - \Omega_{12}\left(X_1^f\right)^2 - RT\ln\left(X_2^f\right) + m_2^{0,B} + \Omega_{12}\left(X_1^B\right)^2 + RT\ln\left(X_2^B\right) \end{pmatrix} = 0 \tag{6.11}$$

This can be simplified to

$$\frac{\Delta G'}{RT} + \ln\left(X_1^f\right) - \ln\left(X_1^B\right) - \ln\left(X_2^f\right) + \ln\left(X_2^B\right) = 0 \tag{6.12}$$

where

$$\Delta G' = \begin{pmatrix} \Delta G^0 - \Omega_{12}\left(1 - X_1^B\right)^2 + \Omega_{12}\left(X_1^B\right)^2 \\ +\Omega_{12}\left(1 - X_1^f - X_3^f\right)^2 - \Omega_{12}\left(X_1^f\right)^2 \end{pmatrix} \tag{6.13}$$

as well as all the interaction parameters.

From eq. (6.12) follows that

$$\frac{\Delta G'}{RT} = \ln\frac{\left(X_1^f\right)\left(X_2^B\right)}{\left(X_2^f\right)\left(X_1^B\right)} \tag{6.14}$$

By taking the exponential functions both sides

$$\exp\left(\frac{\Delta G'}{RT}\right) = \frac{\left(X_1^f\right)}{\left(X_2^f\right)} \cdot \frac{\left(X_2^B\right)}{\left(X_1^B\right)} \tag{6.15}$$

Substituting eq. (6.7) and eq. (6.8) into eq. (6.15), to remove the concentration of the matrix element, it follows that

$$\exp\left(\frac{\Delta G'}{RT}\right) = \frac{\left(X_1^f\right)}{\left(1 - X_1^f - X_3^f\right)} \cdot \frac{\left(1 - X_1^B\right)}{\left(X_1^B\right)} \tag{6.16}$$

$$\frac{\left(X_1^f\right)}{\left(1 - X_1^f - X_3^f\right)} = \frac{\left(X_1^B\right)}{\left(1 - X_1^B\right)} \exp\left(\frac{\Delta G'}{RT}\right) \tag{6.17}$$

where $\Delta G'$ the effective segregation energy.

Using eq. (6.17) to calculate the effect of effective surface segregation energy on surface concentration and the effect of bulk concentration on effective surface segregation energy figure 6.18, figure 6.19 and figure 6.20 can be obtained.

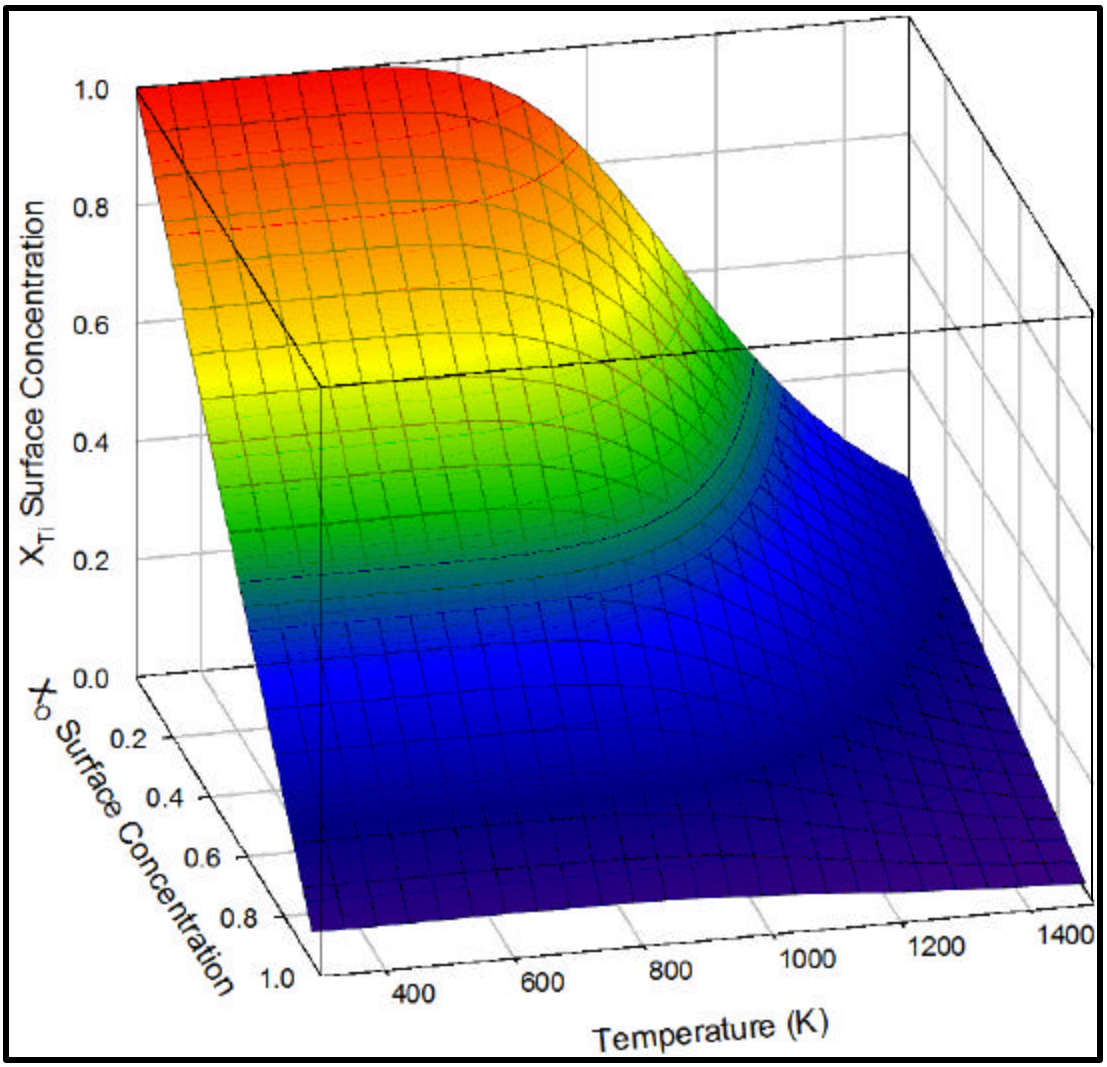

Figure 6.18: Calculated data to shows the effect of the surface concentration for various temperatures on segregation energy.

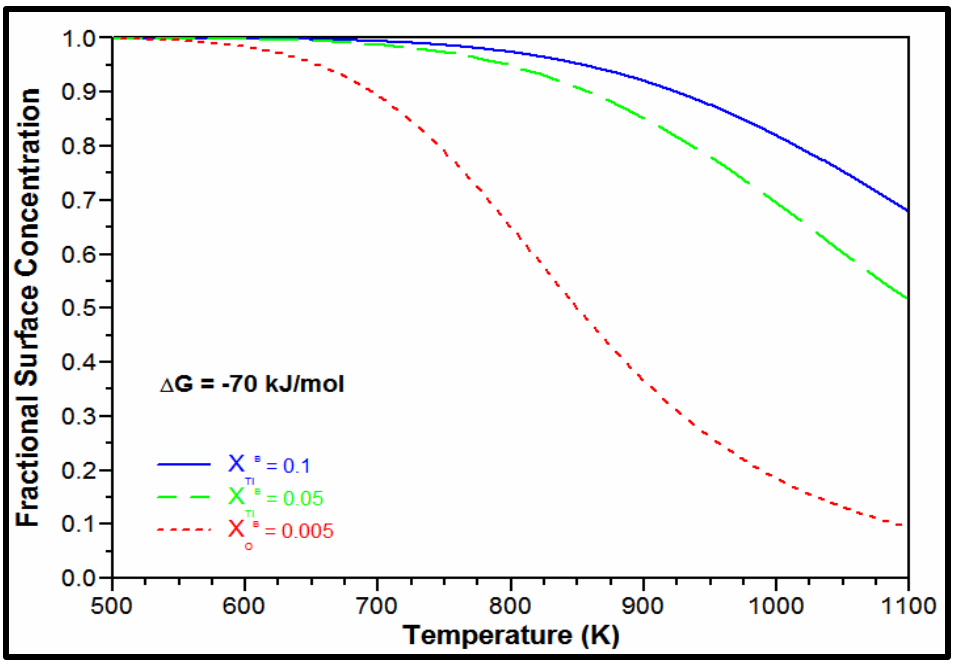

Figure 6.19: Calculated data to show the effect that fractional bulk concentration has on the surface concentration for various temperatures.

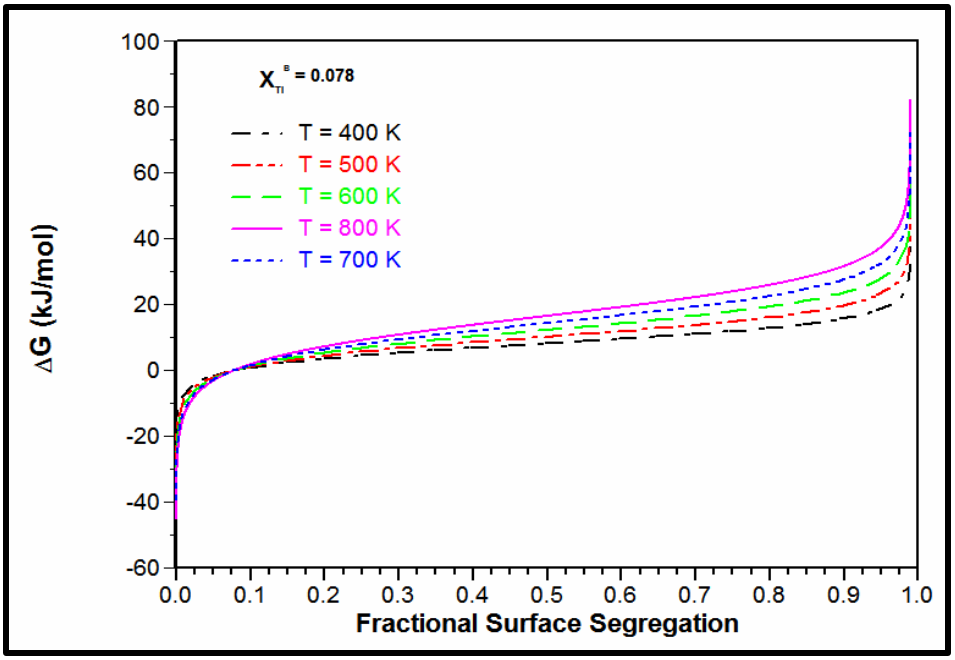

Figure 6.20: Calculated data to show the effect temperature has on the segregation energy at a certain surface concentration.

6.8 Changes in Segregation Energy

For the model a few approximations must be set. Firstly the system is simplified to a binary system with oxygen and additional specie as discussed in the previous sections. Secondly the high rate of titanium segregation initially without any oxygen in the system versus lower rate of segregation with the oxygen in the system, it can be said that the system is at equilibrium the whole time.

The first approximation let the model only set a trend, with small variations in the results, because with an ULC industrial steel the effect of every element plays a crucial role.

The second approximation is only valid at high enough temperatures. Only if this approximation is true the Langmuir-McClean equations can be used as discussed in chapter 3 and 6.

$$\frac{\left(X_1^f\right)}{\left(1-X_1^f-X_3^f\right)}=\frac{\left(X_1^B\right)}{\left(1-X_1^B\right)}\exp\left(\frac{\Delta G'}{RT}\right). \tag{6.18}$$

This equation can now be rewritten for the Ti-Fe system

$$\frac{\left(X_{Ti}^f\right)}{\left(1-X_{Ti}^f-X_{O_2}^f\right)}=\frac{\left(X_{Ti}^B\right)}{\left(1-X_{Ti}^B\right)}\exp\left(\frac{\Delta G_{Ti}'}{RT}\right) \tag{6.19}$$

where X_{Ti}^f the measured fractional concentration of Ti on the surface, $X_{O_2}^f$ the measured fractional concentration of O on the surface, X_{Ti}^B the fractional concentration of Ti in the bulk as obtained from the steel information sheet, T the

temperature of the system (1073 K in this study) and ΔG_{Ti}' the effective segregation energy of Ti as a function of O surface coverage .

In figure 6.21 for the calculated ΔG_{Ti}' from the Langmuir-McClean equations, eq. (6.19) is displayed.

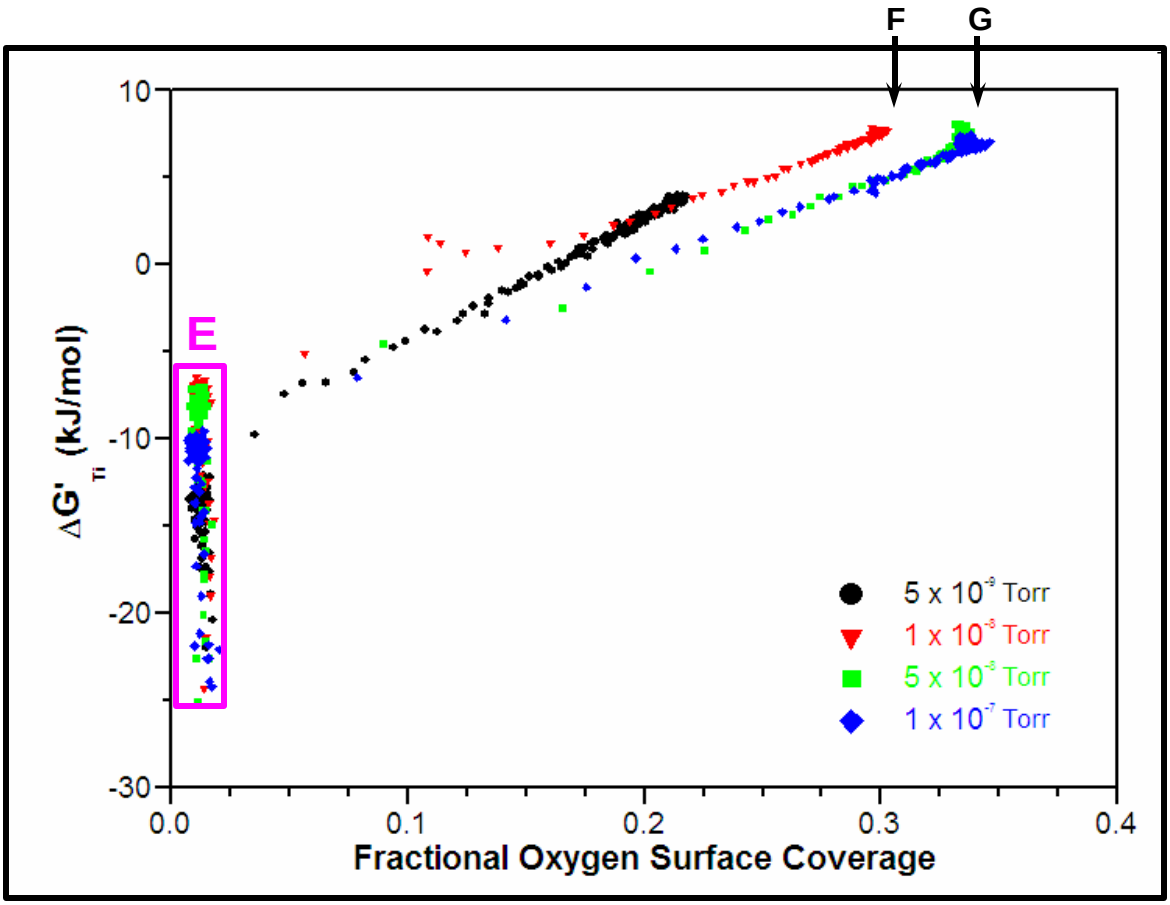

Figure 6.21: Calculated ΔG_{Ti}' ***versus*** $X_{O_2}^{f}$ ***for the different spectra.***

From figure 6.21 the data may be split into two parts, the first part (shown by region E), where no oxygen is present in the system. The second part, illustrated by the data points in a straight line, where oxygen was introduced into the system.

The first region the effective segregation energy is scattered, which can be due to the P concentration on the surface, but the most concentrated at a negative value. The negative value for the segregation energy indicates that Ti will segregate to the surface.

The introduction of oxygen into the system changed the segregation energy linearly to a maximum positive value of 7,9 kJ/mol for the set of pressures. The positive value shows that Ti desegregates from the surface. The segregation energy for the oxygen pressure of 5 x 10^{-9} Torr was lower, due to the P concentration that stayed on the surface. The small fluctuation must be due to P and S which may play a crucial role in the oxidation process. The linear part of 5 x 10^{-8} Torr and 1 x 10^{-7} Torr stayed the same due to the oxygen profiles that stayed constant as seen in figure 6.14, which indicates a saturated system.

The ΔG_{Ti}' maximum value stayed constant for the most pressures at different oxygen coverage values. The difference in oxygen surface coverage of position F and position G was caused by the difference in the TiC and TiO concentration difference illustrated in figure 6.13.

The model predicted that Ti will desegregate, thus the experiment was repeated for a longer period of time, to investigate how good the models predictions were. The obtained data is shown in figure 6.22.

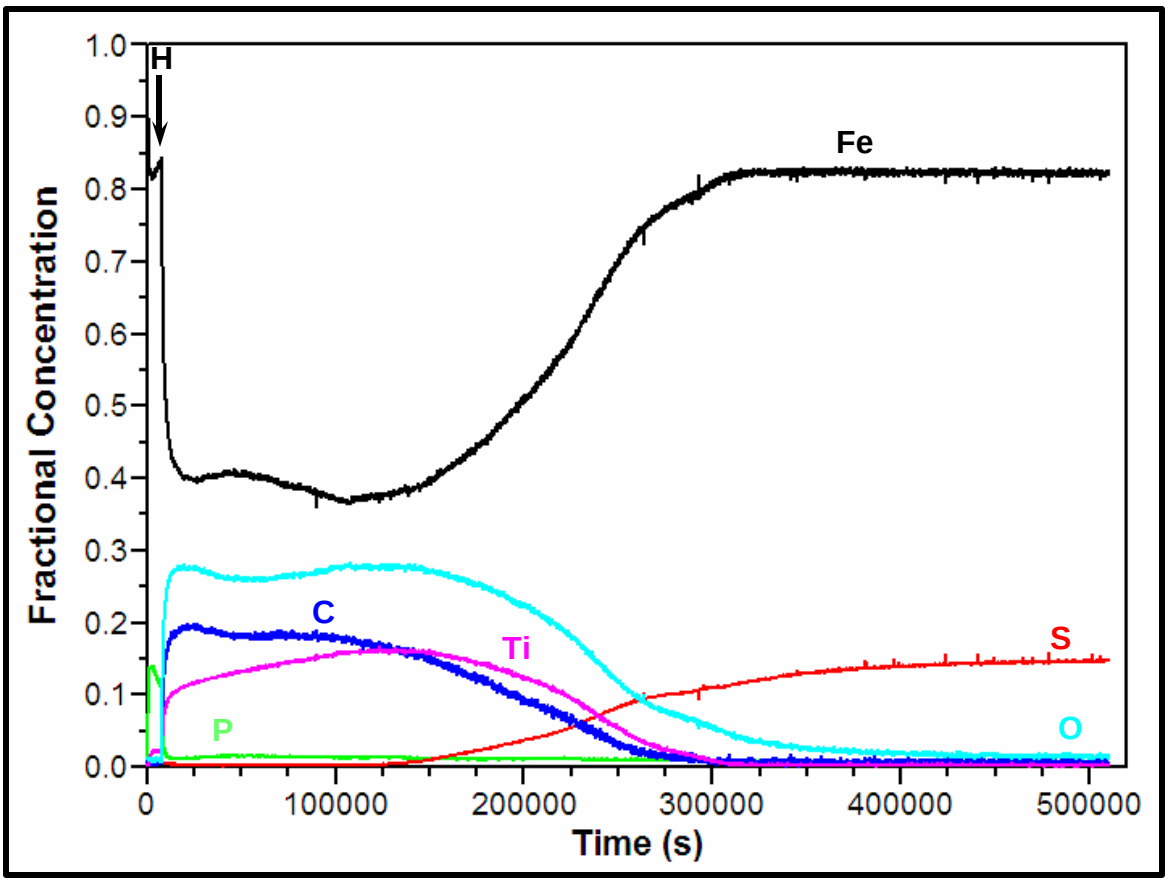

Figure 6.22: Fractional surface concentration versus annealing time at a temperature of 800°C for an oxygen pressure of 5 x 10^{-8}Torr.

In figure 6.22, oxygen was introduced at position H and kept constant. After Ti segregated and reached a maximum the Ti concentration decreased, until no Ti was on the surface, as the model predicted. The possibility of N segregation is not excluded as seen in the increase of the Ti peak. C also followed the same basic profile. The S started to segregate with the decrease of Ti on the surface and forced the oxygen from the surface. The Fe increased with the decrease in the other elements.

This method is a good approximation for the change in effective segregation energy.

Chapter 7

Conclusion

Ti, S and C segregated to the surface of the industrial steel that was used in this study. The complex segregation behaviour during annealing of industrial steel was simulated by the modified Darken model. The initial changes in APPH's of the segregating species against annealing time are comparable with the trends in the surface concentration changes as describe by the Darken model. It was further showed that C and Ti segregation only occurred in the presence of O_2 on the surface. Oxygen-induced segregation of Ti and C occurred at temperatures above 700^{o}C. The concentration changes on the surface during the segregation process depends on the interaction force among the diffusion species and also between the diffusion specie and the bulk atoms, the bulk concentration of the species, the segregation energy of the specie, the temperature and the mobility of the species involved.

A model was proposed for oxygen-induced segregation, using the modified Bragg-Williams equations. The model also showed a way to determine the effective segregation energy as a function of oxygen surface coverage. The model was used to do predictions on the system. It is clear for this study that the segregation and oxidation process involved in the batch annealing is a very complicated process and definitely needs more investigation

7.1 Possible Future Research

In this study the effect of oxygen on segregation was introduced through the oxygen induced segregation of Ti in the industrial steel. An effort was made to see if it is possible to simulate the obtained experimental data. The problem is that with an industrial sample there are so many unknown factors that can play a role during the segregation processes.

In future the model can be improved by simplifying the problem by using an Fe single crystal with a single impurity in it for example Ti. This can be done for different gas atmospheres and the influence of S and P can also be investigated.

References

1. Zylla P, United States Patent-Patent Number:5344509, September 6, (1994)

2. Leroy V and Bouquegneau D, Industry News, May (1999).

3. Lui J, Lu JP, Chu PW and Blakely JM, J. Vac. Sci. Technol, A **10** (1992) 2355.

4. DeArdo AJ, Physical Metallurgy of Interstitial-Free Steels: Precipitates and Solutes, IF Steels 2000 Proceedings (2000) 125.

5. Hubert RA, Dupuis G and Taillard R, Precipitation Reaction in Ti-IF steels: A Comparison between Austenite and Ferrite, IF Steels 2000 (2000) 45.

6. Carabajar S, Merlin J, Massardier V and Chabanet S, Material Science and Engineering A, **281** (2000) 132.

7. Cabibil H and Kelber JA, Surf. Sci., **329** (1995) 101.

8. Holtzhausen DJ and Roux JP, Corr. Sci., **30** (1990) 67.

9. Tjong SC and Swart HC, Appl. Surf. Sci., **47** (1991) 311.

10. van Staden MJ and Roux JP, Appl. Surf. Sci., **44** (1990) 263.

11. McMahon CJ, Jr. and Marchut L, J. Vac. Sci. Technol., **15(2)** (1978) 450.

12. du Plessis J and van Wyk GN, J. Phys. Chem. Solids, **49** (1988) 1442

13. du Plessis J, Surface Segregation, Solid State Phenomena, Diffusion and Defect Data, **11** (1990) 67

14. du Plessis J and Viljoen EC, Appl. Surf. Sci., **100/101** (1996) 222

15. Guttmann M, Surface Science, **53** (1975) 213.

16. Ramsey MG and Russel GJ, Phys. Rev. B, **30** (1984) 6960

17. Lupis CHP, Chemical Thermodynamics of Materials, North-Holland, Amsterdam, (1983)

18. Askeland DR, The science and engineering of materials, Third Edition, Stanley Thornes Publishers Ltd., Cheltenham, (1996)

19. Shewmon PG, Diffusion of Solids, McGraw-Hill Book Company, (1963)

20. du Plessis J, van Wyk GN, J. Phys. Chem. Solids, **50** (1989) 237

21. du Plessis J, Viljoen PE, van Wyk GN, Surface Science, **244** (1991) 277

22. Joubert HD, A Monte Carlo program for simulating segregation and diffusion utilizing chemical potential calculations, MSc Thesis, University of the Free State, South Africa, (2004)

23. Terblans JJ, Erasmus WJ, Viljoen EC, du Plessis J, Surf. Interface Anal., **22** (1999) 70

24. Terblans JJ, Modelling and experimental investigation of Sb-surface segregation in Cu-single crystals, PhD Thesis, University of the Free State, South Africa, (2001)

25. Erasmus WJ, Die segregasie van Sb na die lae indeksoppervlakke van Cu enkelkristalle, MSc Thesis, University of the Free State, South Africa, (1999)

26. Glossary of Chemical Terms, Weizmann Institute of Science (Online), (***http://www.weizmann.ac.il/safety/chgl.html***). Date accessed 7 November 2005

27. Hoffmann S, Thin Solid Films, **193/194** (1990) 648

28. Isaacs A, Dictionary of Physics, Fourth Edition, Oxford University Press, Oxford, (2000)

29. Zangwill A, Physics at Surfaces, Cambridge University Press, Cambridge, (1988)

30. Bond GC, Heterogeneous Catalysis: Principles and Applications, Clarendon Press, Oxford, (1974)

31. Cottrell A, An Introduction to metallurgy, Second Edition, Edward Arnold Publishers Ltd., London, (1975)

32. Fromhold AT, Theory of metal oxidation, North-Holland Publishing Company, New York, (1976)

33. Birks N and Meier GH, Introduction to high temperature oxidation of metals, Edward Arnold Publishers Ltd., London, (1983)

34. Kubaschewski O, Iron – Binary Phase Diagrams, Springer-Verslag, New York, (1982)

35. Tretheway KR and Chamberlain, Corrosion for students of science and engineering, Longman Scientific & Technical, New York, (1990)

36. McMahon CJ, Marchut L, J. Vac. Sci. Technol, **15** (1978) 455

37. Walls JM, Methods of surface analysis, Cambridge University Press, Cambridge, (1989)

38. Briggs D and Seah MP, Practical Surface Analysis – Volume 1, Second Edition, John Wiley & Sons Ltd., Chichester, (1990)

39. Swart HC, Jonker AJ, Claassens CH, Chen R, Venter LA, Ramoshebe P, Wurth E, Terblans JJ and Roos WD, Applied Surface Science, **205** (2003) 231

40. Hedberg CL, Handbook of Auger Electron Spectroscopy, Third Edition, Physical Electronics Inc., Eden Prairie, (1995)

41. Greeff AP, Die oksidasie van industriële FeCrMo staal, MSc Thesis, University of the Free State, South Africa, (1999)

Conference Contributions

National

Impurity segregation during batch annealing of industrial steel coils

E Wurth, JJ Terblans, CJ Greyling and HC Swart

SAIP Conference 2002

The influence of oxygen pressure on oxygen induced surface segregation

E Wurth, JJ Terblans, CJ Greyling and HC Swart

SAIP Conference 2003

Suurstof-geïnduseerde segregasie tydens uitgloeiing van industriële staal

E Wurth, JJ Terblans, CJ Greyling and HC Swart

Studente Simposium 2003

Oxygen-induced segregation during batch annealing of industrial steel coil

E Wurth, JJ Terblans, CJ Greyling and HC Swart

SAIP Conference 2004

An improved heater system for high-temperature Auger electron spectroscopy

E Wurth, AB Hugo, HC Swart, WD Roos and JJ Terblans

SAIP Conference 2005

The effect of absorbed oxygen on the segregation energy of Ti

E Wurth, JJ Terblans and HC Swart

SAIP Conference 2006

International

Oxygen-induced segregation during batch annealing of industrial steel coils

E Wurth, JJ Terblans, CJ Greyling and HC Swart

IWSIS 2003